Chem Soc Rev

REVIEW ARTICLE

View Article Online
View Journal | View Issue

Cite this: *Chem. Soc. Rev.*, 2023, **52**, 2497

Ionogels: recent advances in design, material properties and emerging biomedical applications

Xiaotong Fan,†[a] Siqi Liu,†[c] Zhenhua Jia,[be] J. Justin Koh,[d] Jayven Chee Chuan Yeo,[d] Chen-Gang Wang,[a] Nayli Erdeanna Surat'man,[a] Xian Jun Loh,[ad] Jean Le Bideau,*[f] Chaobin He,*[cd] Zibiao Li*[acd] and Teck-Peng Loh*[be]

Received 13th September 2022

DOI: 10.1039/d2cs00652a

rsc.li/chem-soc-rev

Ionic liquid (IL)-based gels (ionogels) have received considerable attention due to their unique advantages in ionic conductivity and their biphasic liquid–solid phase property. In ionogels, the negligibly volatile ionic liquid is retained in the interconnected 3D pore structure. On the basis of these physical features as well as the chemical properties of well-chosen ILs, there is emerging interest in the antibacterial and biocompatibility aspects. In this review, the recent achievements of ionogels for biomedical applications are summarized and discussed. Following a brief introduction of the various types of ILs and their key physicochemical and biological properties, the design strategies and fabrication methods of ionogels are presented by means of different confining networks. These sophisticated ionogels with diverse functions, aimed at biomedical applications, are further classified into several active domains, including wearable strain sensors, therapeutic delivery systems, wound healing and biochemical detections. Finally, the challenges and possible strategies for the design of future ionogels by integrating materials science with a biological interface are proposed.

[a] *Institute of Sustainability for Chemicals, Energy and Environment (ISCE²), Agency for Science, Technology and Research (A*STAR), 1 Pesek Road, Jurong Island, Singapore 627833, Singapore. E-mail: lizb@imre.a-star.edu.sg*

[b] *College of Advanced Interdisciplinary Science and Technology, Henan University of Technology, Zhengzhou, 450001, P. R. China. E-mail: teckpeng@ntu.edu.sg*

[c] *Department of Materials Science & Engineering, National University of Singapore, 9 Engineering Drive 1, Singapore 117575, Singapore. E-mail: msehc@nus.edu.sg*

[d] *Institute of Materials Research and Engineering, Agency for Science, Technology and Research (A*STAR), 2 Fusionopolis Way, Singapore 138634, Singapore*

[e] *Division of Chemistry and Biological Chemistry, School of Physical and Mathematical Sciences, Nanyang Technological University, Singapore, 637371, Singapore*

[f] *Nantes Université, CNRS, Institut des Matériaux de Nantes Jean Rouxel, IMN, F-44000 Nantes, France. E-mail: Jean.LeBideau@cnrs-imn.fr*

† X. F and S. L contributed equally to this work.

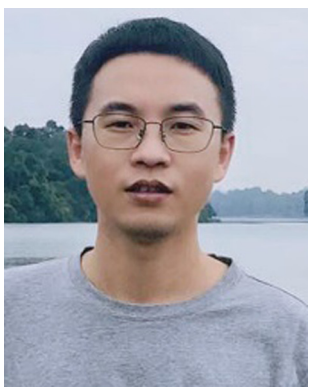

Xiaotong Fan

*Dr Xiaotong Fan obtained his PhD majoring in Polymer Chemistry and Physics from Jilin University, China. After that, he became a research fellow at Materials Science and Engineering in the National University of Singapore (NUS). He is currently working as a research scientist at the Institute of Sustainability for Chemicals, Energy and Environment (ISCE²), Agency for Science, Technology and Research (A*STAR), Singapore. His current research interests focus on the design of ionogels, functional polymers, and biopolymers for biomedical applications.*

Zhenhua Jia

Zhenhua Jia is a full professor at the College of Advanced Interdisciplinary Science and Technology, Henan University of Technology. He received his BS in 2004 from Tianjin University and PhD in 2013 from Sun Yat-sen University and joined McGill University under the supervision of Prof. Albert S. C. Chan and Prof. Chao-Jun Li. Then he continued to pursue his postdoctoral research at Marquette University, Chinese University of Hong Kong and University of Alberta with Prof. Chae S. Yi, Prof. Henry N. C. Wong, and Prof. Frederick G. West, respectively. In 2018, he joined Prof. Teck-Peng Loh's team and hold his current position. His research interest includes green and sustainable synthesis, and organic transformations under biocompatible conditions.

1. Introduction

Gels are a class of materials containing three-dimensional polymeric networks that can support plenty of solvents. Cross-linking junctions can be formed by covalent bonds or non-covalent interactions, such as metal coordination, hydrogen bonding, host–guest interactions, ionic association, and hydrophobic interactions.[1–3] The source of polymers can be synthetic or natural, whose structure and properties will greatly affect the properties and applications of gels. According to the used dispersion medium, gels are usually classified into organogels, hydrogels, oleogels, and ionogels, depending on whether they are mainly composed of organic solvents, water, oil, and ionic liquids, respectively.[4] Although gels have been employed in many fields, such as actuators, soft electronics, water treatment, energy, and wound healing,[5–7] their drawbacks such as easily drying out for hydrogels and toxicity for organogels caused by the nature of organic solvents limit their wider applications. In recent years, ionic liquid (IL)-based gels as new advanced gels have aroused considerable attention due to the advantages of chemical, thermal and electrochemical stability, non-volatility and non-flammability.

Ionogels are gel materials consisting of ILs as the dispersed phase immobilized by organic or inorganic networks as the

Jean Le Bideau

Jean Le Bideau is a professor at Institut des Matériaux de Nantes Jean Rouxel (IMN), at Nantes University. He is a principal investigator for research on ionogels and hydrogels. His current research focuses on the effect of the chemical and topological nature of the confining network on the dynamics of the confined liquid. The fields of applications more particularly targeted are electrochemical energy storage and tissue engineering for regenerative medicine.

Chaobin He

*Chaobin He received his PhD degree from the Department of Materials Science and Metallurgy, University of Cambridge in 1995. After graduation, he worked in Cavendish Laboratory, University of Cambridge, as a postdoctoral associate for two years and later at the University of Southern Mississippi, USA, for another two years before he joined the Institute of Materials Research and Engineering (IMRE) under A*STAR in 1999. Currently, Dr He is an associate professor in the Department of Materials Science and Engineering, National University of Singapore, and holds a joint-appointed position as a Principal Scientist at IMRE. His current research interests are in the areas of polymer nano-structured materials, organic–inorganic hybrid materials, and block copolymers and self-assembly.*

Zibiao Li

*Zibiao Li is the director of the Sustainable and Green Materials Division at the Institute of Sustainability for Chemicals, Energy and Environment (ISCE^2), Agency for Science, Technology and Research (A*STAR), Singapore. Li holds a joint appointment at the Institute of Materials Research and Engineering (IMRE) and is an adjunct associate professor at the National University of Singapore (NUS). His research interests focus on materials sustainability and MedTech polymers for healthcare applications.*

Teck-Peng Loh

Teck-Peng Loh is a distinguished university professor of Chemistry at Nanyang Technological University, Singapore. Under the tutelage of Professor E. J. Corey, he obtained his PhD (1994) from Harvard University. He has been awarded outstanding researcher awards from both the National University of Singapore and Nanyang Technological University. In 2017, he received the Yoshida Prize (Japan) and the prestigious President's Science Award (individual) in Singapore. He has been elected Fellow, Academia of Sciences, Singapore (2018), and Fellow of the Academia of Sciences, Malaysia, since 2010. His research work mainly focuses on the development of new synthetic methodology, green chemistry, and the synthesis of natural and unnatural products.

matrix. Since the first reports of IL-based gels with either organic or inorganic host networks in 2005,[8,9] much effort has been dedicated to the research on IL-based gels, which have been applied in many fields, such as energy storage, bioelectronics, sensors, and actuators.[10–14] Among these reported works, several naming systems have been found, such as ionic liquid gels,[15] ionogels,[16] ion gels,[17,18] ion-gels[19] and iongels,[20] which make it difficult to reference. In this review, we will adapt ionogels as the name. The network matrices in ionogels can be organic, for example, polymers and small molecules, or inorganic, for example, SiO_2 and TiO_2. One of their main advantages is their biphasic feature, where the solid host network confines a major part of the liquid. Due to the numerous IL types and various network matrices, the possible combinations for fabricating ionogels are infinite, resulting in the components and properties of ionogels being variable. According to the desired applications, researchers can construct ionogels using different strategies.

While several excellent reviews on ionogels have been published,[10,21,22] reviews especially focusing on ionogels for biomedical applications are in urgent demand.[23] Therefore, it is necessary to summarize the latest advances to provide insights into the development trends of ionogels in this research area. In this review, the latest achievements in ionogels for biomedical applications are highlighted. Besides presenting the current preparation procedures and processing methods for ionogels, some of the key properties of ionogels, such as ionic conductivity, thermal stability, and electrochemical stability, are introduced, followed by the emerging applications of ionogels in various biomedical areas (Fig. 1).

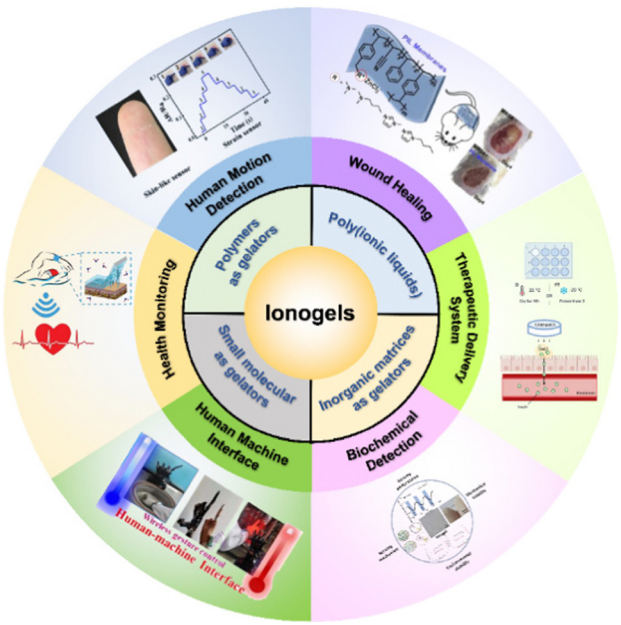

Fig. 1 Preparation methods of ionogels and the emerging biomedical applications. Adapted with permission from ref. 24 Copyright 2021, Elsevier; ref. 25 Copyright 2019, American Chemical Society; ref. 26 Copyright 2020, American Chemical Society; ref. 27 Copyright 2022, Elsevier; ref. 28 Copyright 2022, Elsevier; ref. 29 Copyright 2021, John Wiley & Sons, Inc.

2. Types of ionic liquids

In general, ILs can be categorized into protic ILs and aprotic ILs. Protic ILs are a subset of ILs that contain an available proton on the cations, and aprotic ILs are those that contain no available proton on the cations.[30–33] Protic ILs are produced through the combination of a Brønsted acid and a Brønsted base.[30,34] The resultant charged species is a consequence of proton transfer from the Brønsted acid to the Brønsted base, as shown in Fig. 2A. In fact, the first IL discovered, ethylammonium nitrate (EAN),[35] was a protic IL with a melting temperature (T_m) of ~12 °C, which is also one of the most extensively studied IL. EAN can be easily synthesized by reacting ethylamine with concentrated nitric acid, also illustrated in Fig. 2A. In reality, proton transfer between the two originally neutral acid and base species may be incomplete, leading to the existence of neutral species in the system. This issue can possibly be improved by using stronger acids and/or bases, using their pK_a values as an indication, even though pK_a values are usually considered for only aqueous systems.

While protic ILs can be made simply by mixing already synthesized acid and base, the production of aprotic ILs usually has to go through a longer synthesis route. Typical/traditional synthesis of aprotic ILs starts from alkylation of the corresponding amine, phosphine or sulfide of interest, *via* alkyl halides (R–X), leading to the formation of halide salt with the desired cation.[31] This halide salt itself can be considered IL if it possesses a sufficiently low melting point of <100 °C. Nevertheless, to pair the cation with a desired organic anion instead of the halide, the anion exchange can be carried out through a metathesis process.[36] This generic synthesis route is illustrated through the synthesis of imidazolium aprotic ILs with $[TFSI]^-$ as the anion and 1-methylimidazole as the precursor, which is presented in Fig. 2B.

The most common families of cations in ILs are shown in Fig. 3. They include imidazolium, pyridinium, piperidinium, pyrrolidinium and ammonium. Other than the aforementioned

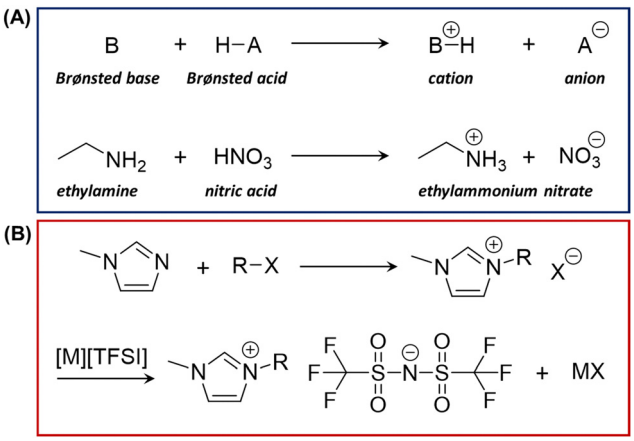

Fig. 2 (A) Typical synthesis of protic ILs through neutralization reaction between a Brønsted acid and a Brønsted base. The synthesis of ethylammonium nitrate is provided as an example. (B) Typical synthesis route of aprotic ILs, using imidazolium-based ILs with $[TFSI]^-$ anion as an example.

ILs based on charged nitrogen, phosphorous-based phosphonium and sulfur-based sulfonium are also common.[37] These families of cations form both protic ILs and aprotic ILs.[38] Similarly, some common anions are also presented in Fig. 3. Typical inorganic ones include halides ($[Cl]^-$, $[Br]^-$, $[I]^-$), $[NO_3]^-$, $[BF_4]^-$, $[PF_6]^-$ and $[HSO_4]^-$. Typical organic ones include $[DCA]^-$, carboxylates such as $[Ac]^-$, sulfates such as $[EtSO_4]^-$, sulfonates such as $[MeSO_3]^-$, phosphates such as $[DEP]^-$, phosphonates such as $[MeO(H)PO_2]^-$, as well as fluorinated ones, such as $[TFSI]^-$, $[FSI]^-$ and $[OTf]^-$. Considering the different combinations of cations and anions, the types of ILs are various, and some unique properties of ILs can be observed. ILs have been applied in different areas, including catalysis,[39] electronics,[40] energy storage,[41] and biotechnology.[42] Our group has described the applications of ILs in organic synthesis since 2002. Replacing conventional solvents, the unique reactivity and selectivity of ILs were exhibited in various polar reactions.[43–59]

According to the chemical structures and properties, ILs can be classed into three generations (Fig. 4). First-generation ILs typically consist of dialkylimidazolium or alkylpyridinium cations with chloroaluminate(III) (*e.g.* $[AlCl_4]^-$) and other metal halide anions (*e.g.* $[FeCl_4]^-$).[60–63] However, these compounds are highly water/moisture sensitivity, they have to be handled in an inert environment. The most significant development of second-generation ILs is the replacement of the anions with relatively stable $[BF_4^-]$ and $[PF_6^-]$, as well as halides and carboxylates.[64] While dialkylimidazolium cations remain popular through ILs' development, highly utilized cations expanded to include phosphoniums and ammoniums. While the objective for the development of second-generation ILs is to improve their stability, there is no general consensus on the specific goal of third-generation ILs. Some authors have identified third-generation ILs to be "task-specific" ILs (TSILs)[61,65] as proposed by Davis.[66] This is largely due to the broadening of ILs' applicability beyond solvents including catalysis, biomedical, electronics and energy storage applications. However, many of the "improved" designs/modifications of ILs become beneficial for a single field and not exactly an overall progress of ILs as a whole. In fact, the unique characteristics of third-generation ILs can be observed from the bulk of the research that aims to resolve some major shortcomings of the second-generation ILs, such as toxicity and non-sustainability. Therefore, characteristics such as low

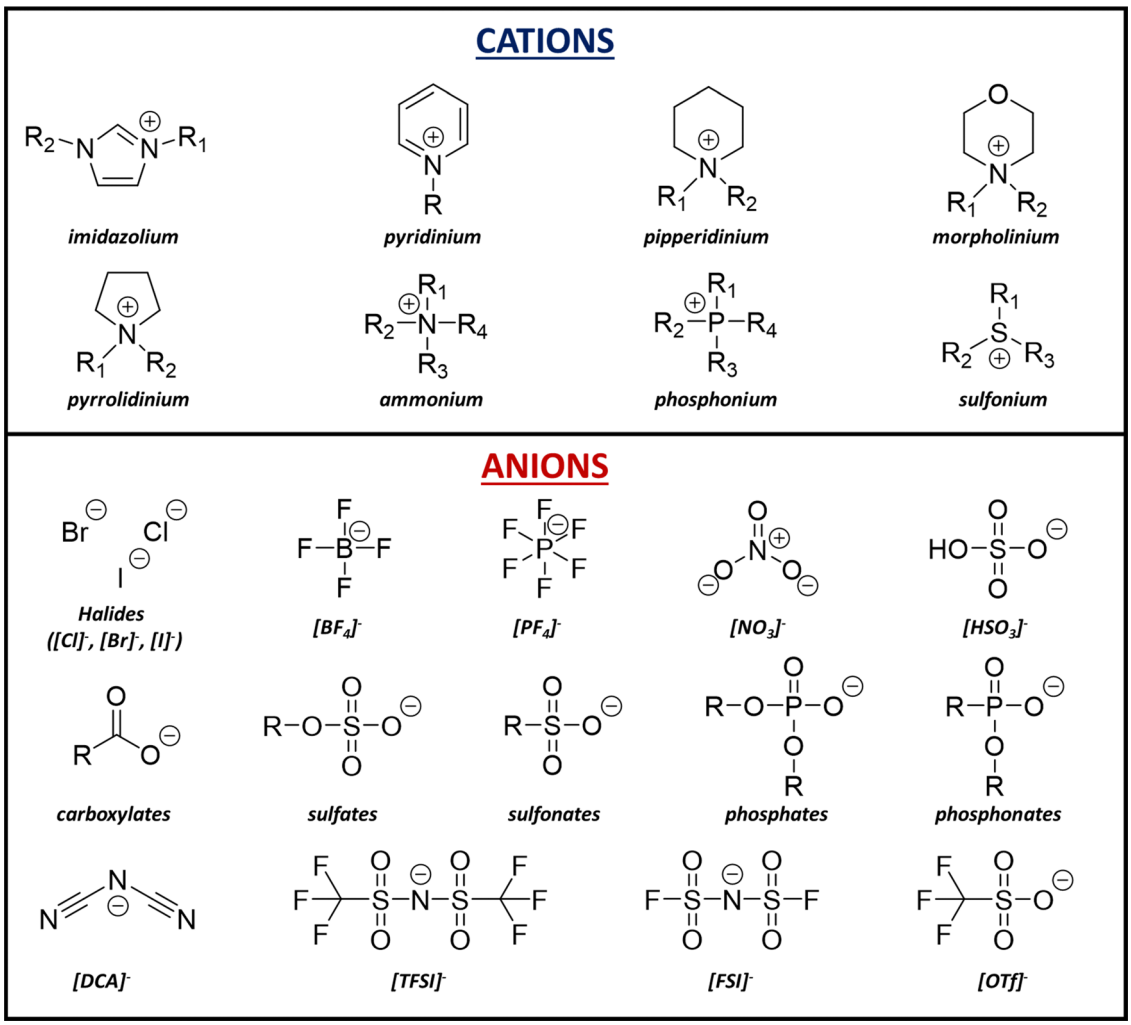

Fig. 3 Common cations and anions of ILs. R represents the typical substitution sites, R = H or alkyl.

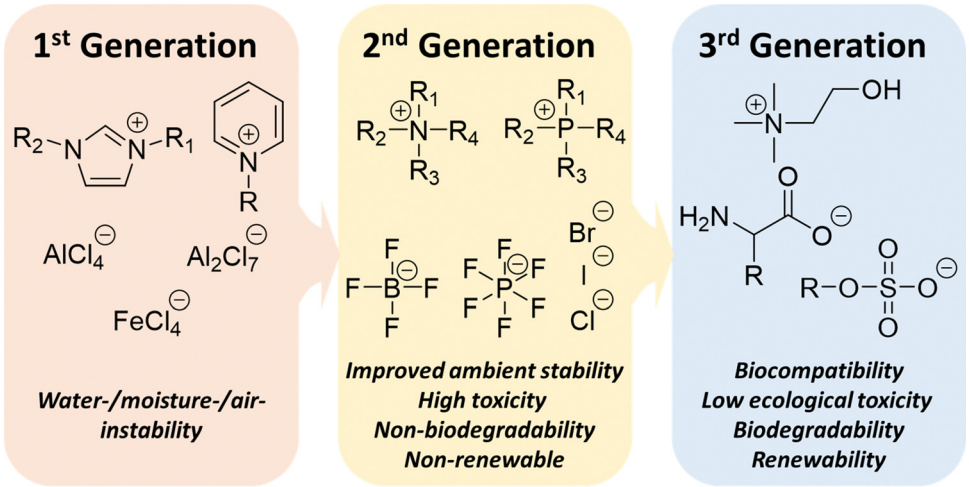

Fig. 4 Different generations of ILs.

ecological toxicity, biocompatibility, biodegradability and renewability are highly beneficial properties, regardless of the wide range of IL applications. This definition is also similar to that defined by Egorova *et al.*[67] and Gorke *et al.*[68] For instance, naturally occurring cations such as cholinium and anions such as amino acids, sugars/modified sugars and alkylsulfates are important developments of third-generation ILs.[69–76] The emergence of the third-generation ILs provides the possibility of their application in the biomedical field.

2.1. Physicochemical properties of ionic liquids

This section will highlight some key physicochemical properties of ionic liquids that set them apart from other chemical substances. As the name suggests, ILs are substances that contain electrically charged (ionic) species in the liquid state. Therefore, the discussion will focus on the charged and liquid aspects that allow ILs to possess a unique character.

While not all of the ILs are liquid at room temperature, for instance $[EMIM]^+[Cl]^-$ has a T_m of $\sim$87 °C,[77] the general consensus in the scientific community is that they should possess a low T_m of less than 100 °C,[30] even though there is nothing really special about the 100 °C mark, except that it is the boiling point (T_b) of water. Nevertheless, this also gives rise to the term, room-temperature ionic liquids (RTILs),[78] so as to classify ILs that are already in a liquid state at room temperature. Despite the strong electrostatic interactions between the positively and negatively charged species, the low T_m of ILs as compared to other salts, for example, table salt (T_m $\sim$ 801 °C) can be attributed to the large size of the cation and/or the anion, along with the low symmetry of the heterocyclic cations. In fact, for some ILs, T_m is absent and the substance undergoes glass transition at very low temperatures.[79] These thermal transition temperatures are key properties that determine the operation temperature of these ILs, as well as differentiating ILs from other salt substances.

As compared to ordinary liquids that typically consist of electrically neutral molecules, ILs are made up of electrically charged ions. The strong coulombic attraction between the cations and anions would lead to coulombic compaction, whereby the volume of the liquid is reduced, resulting in higher density. A study that compares 1-methoxyethylpyridinium dicyanamide and its neutral isoelectronic analog, a binary solution of 1-methoxyethylbenzene and dicyanomethane, shows that the IL is about 20% denser.[80] Similarly, ILs are generally much more viscous than water and common organic solvents, and it is also known that the density of a liquid has a positive effect on its viscosity.[81] However, another recent study involving triethyl(3-methoxypropyl)phosphonium butyrate and its neutral analog of triethyl(3-methoxypropyl)silane and 1-nitropropane binary mixture[82] shows that the IL still has a viscosity of about sixteen times that of the neutral binary solution despite being under isodensity conditions (by applying high pressure to neutral analog). More importantly, as a direct consequence of the electrostatic interactions, the vapor pressure of ILs is known to be extremely low. Though initially thought to be inconsequential, ILs can exhibit measurable vapor pressure under reduced pressure or elevated temperatures.[32,83]

With mobile charge carriers, ILs are definitely better electrical conductors than solid salts and electrically neutral organic liquids. However, the electrical conductivity, or more specifically, the ionic conductivity of ILs is limited mainly by two factors: large ion size and high viscosity.[84,85] Despite the increase in density from the coulombic compaction effect, the large molecular size of the cations and anions would limit the number of charge carriers per unit volume. Furthermore, as discussed, ILs are typically viscous fluids. Since ion mobility is inversely related to viscosity, ionic conductivity is also limited by this. Other factors such as the occurrence of ion aggregates may also affect the ionic conductivities. As such, the ionic conductivities can reach up to around 10 mS cm^{-1}, which is generally lower than that of concentrated aqueous electrolytes.[86] The ionic conductivity of ILs could endow ionogels with conductivity, facilitating their usage in the fields of wearable strain sensors and biochemical detection.

Stability in an ambient environment is the majority concern for first-generation of ILs, which are mainly based on chloroaluminate(III) and other metal halide anions.[61] Due to their water/moisture sensitivity, they have to be handled in an inert environment, greatly reducing their practicality. This leads to second-generation ILs that possess relatively less sensitive anions that can be handled in the ambient environment. However, some second-generation ILs are also not exactly water-stable, in particular, $[BF_4]^-$ and $[PF_6]^-$ anions are known to hydrolyze in the presence of water, leading to the formation of highly hazardous and corrosive hydrogen fluoride.[87] Many of the anions that are stable in the presence of moisture/water were subsequently developed, such as bis-(trifluorosulfonyl)-imide $[TFSI]^-$ (Fig. 3). However, many of them are still hygroscopic, and water content can change their physicochemical properties significantly. It has also been reported that the hydrophilicity/hygroscopicity of the IL is largely determined by its anions.[88] For instance, water is miscible with $[EMIM]^+[EtSO_4]^-$ over the concentration range but only has limited solubility in $[EMIM]^+[TFSI]^-$.

For thermal stability, the decomposition onset temperature (T_{onset}) measured by thermogravimetric analysis (TGA) is typically used to characterize the thermal stability of the IL at elevated temperatures.[89] T_{onset} is obtained through the intersection between the initial mass baseline and the tangent to the TGA decomposition curve at maximum gradient. T_{onset} values of ILs are generally high, typically above 250 °C, and sometimes above 400 °C, giving the impression that ILs are of high stability at elevated temperatures.[90] However, significant degradation of ILs can take place at a much lower temperature for an extended period of time. As such, another parameter, $T_{0.01/x}$, which is the temperature at which 1% mass loss due to decomposition occurs in x hours, was proposed to study the thermal degradation of ILs.[91] This would allow better comparison with the real operational temperature range. Indeed, the difference between T_{onset} and $T_{0.01/10}$ can be as large as ~200 °C. The thermal stability of ILs ensures that the ionogel-based devices operate over a wide temperature range, broadening their application scenarios.

ILs generally exhibit a large electrochemical window, typically between 4.5 and 5 V,[92] and up to about 7 V for $[BMIM]^+[BF_4]^-$ and $[BMIM]^+[PF_6]^-$,[93] but such wide electrochemical window has to be thoroughly tested against time. Within the window, oxidation of the anions and reduction of the cations would not occur. In general, such a window is comparable to organic electrolytes and significantly wider than that of aqueous electrolytes.

The excellent properties of high conductivity, thermal stability, and wide electrochemical window make ILs attractive candidates for fabricating advanced functional materials which have special requirements for materials properties of high conductivity, stability, and wide electrochemical window. The ionogels prepared from ILs can perfectly inherit the properties of ILs and will exhibit potential applications in wearable strain sensors and biochemical detection.

2.2. Biological properties of ionic liquids

For ILs to be widely applied in biomedical applications, their cytotoxicity, especially mammalian cell cytotoxicity and biodegradability have to be considered. To estimate the cytotoxicity, usually, the half maximal inhibitory concentration (IC_{50}) or half maximal effective concentration (EC_{50}) was used. In general, the chemical structure of both the cations and anions can affect the cytotoxicity of the IL, some more influential than others. Amongst the molecular structure effect on cytotoxicity, the effect of alkyl length on the cations has been reported to be the most pronounced.[94] The increase in alkyl chain length of cations would typically lead to higher toxicity,[95,96] most possibly due to an increase in the lipophilic character, whereby the strong IL-lipid bilayer interaction would cause disintegration of the lipid bilayer.[97] Nevertheless, the increase in toxicities also appears to be insignificant after a certain alkyl chain length, typically known as the ''cutoff effect''.[98] On the other hand, the effect of different cation head groups on cytotoxicity appears to be lesser as compared to the change in the alkyl chain length. Nevertheless, some trends can be observed, for example, piperidinium-based ILs have been reported to be about 20 times more toxic than pyrrolidinium-based ones,[94] despite pairing with the same anion. On the other hand, pyridinium-based dicationic ILs have been reported to exhibit less cytotoxicity as compared to their monocationic counterparts,[99] possibly due to the alkyl chains being trapped between the two cationic moieties, hence reducing their lipophilic effect. For anions, their effect on cytotoxicity has been considered to be somewhat minimal as compared to cations, though there are still trends that can be considered.[100] For instance, some relatively low toxic anions are $[DEP]^-$ and $[DMP]^-$, while $[NTf_2]^-$ exhibit relatively higher toxicity, presumably due to the increased lipophilicity of the anion.[94]

The anti-bacterial effect of ILs has drawn extensive attention from researchers, as many ILs, for example, pyridinium, imidazolium, and pyrrolidinium, exhibit inhibitory effect on the growth of various bacteria and fungi.[67] From the view of biotechnology, high toxicity may be a serious issue. However, by appropriate assessment and selection, ILs can serve as efficient anti-bacterial agents because of their high toxicity to bacteria and fungi.[101,102] The anti-bacterial activity of ILs can be ascribed to the insertion into the bacterial membrane by alkyl chains as well as the electrostatic interactions between the cationic groups of ILs and bacterial cell walls,[97] leading to bacterial death. Similar to cytotoxicity, the anions are known to play a much smaller role as compared to the effect of the cation's alkyl chain length. ILs with anti-bacterial properties are suggested to be utilized in the fabrication of ionogels, which can inherit the anti-bacterial effect from the corresponding ILs for potential wound healing applications.

A general strategy to synthesize biocompatible ILs (Bio-ILs) is to use natural or biocompatible starting materials[103] such as amino acids, sugars, and carboxylic acids. Among the Bio-ILs, cholinium cations remain highly dominant, initially due to the natural occurrence of choline, an essential nutrient for many animals including humans, therefore postulated to be highly

biocompatible.[104] Studies have found that cholinium cations, when paired with other naturally occurring counterions, such as amino-acid-based or carboxylate-based anions, are largely biocompatible. Similarly, glycine betaine-based cations have also been reported more recently as economical alternatives to cholinium.[105] For amino acids, similar to carboxylic acids, their carboxyl groups can be conveniently utilized to form carboxylates to perform as anions in Bio-ILs.[106] Besides, its amine group can also be used to form cations of protic ILs through protonation with strong acids.[107] In addition, cations of aprotic ILs can also be formed with amino acids through more complex synthetic processes.[108] Sugars can also be modified into sugar acids, such as glucuronic acid and galacturonic acid that contain carboxylate groups to perform as anions. Likewise, sugars can also be modified with substituted side groups that possess positively charged heteroatoms, such as sulfonium or ammonium. The biocompatibility of ILs can make ionogels biocompatible, which is beneficial for the biomedical applications of ionogels.

Despite consisting of at least a pair of cations and anions, ILs are often regarded as a single substance therefore, when considering the biodegradability of ILs, both the cation and anion should be considered.[109] In addition, while the degradability of the cation and anion can be considered separately based on general trends, different counterions can also influence the biodegradation rate of some ions.[110]

For anions, halides (consisting of a single atom) and other inorganic molecules such as $[BF_4]^-$ and $[PF_6]^-$ are not included in the discussion here. One of the first highly biodegradable anions of ILs reported is octyl sulfate,[70] in fact, alkyl sulfates generally exhibit good rates of degradation.[69] Besides, many conjugates based on organic acids, sugar acids and amino acids, typically containing carboxylate charged group, have also been found to be highly biodegradable.[111]

Many of the commonly found cations in ILs turn out to have rather a low biodegradability, including aromatic cations from the imidazolium-,[112] pyridinium-,[113] and thiazolium-family,[69] as well as non-aromatic ones from the pyrrolidinium-,[114] morpholinium-families.[115] Many of the ammonium-family cations appear to be more biodegradable than others. In particular, the cholinium cation, together with its protic analogue (aminodiol and aminotriol derived ILs), is among the most common for the synthesis of biodegradable ILs.[116] The dimethyldibutylammonium (DMDBA) cation also appears to be readily biodegradable when paired with some certain anions, such as $[Ac]^-$ and $[Lac]^-$, but not biodegradable when paired with $[Cl]^-$ anions. In addition, there have also been some successes in chemically modifying some of those cations that are harder to be biodegraded to improve their biodegradability. For example, Gathergood *et al.*[117] reported two readily biodegradable imidazolium-based ILs, using amino acid derived imidazolium as a cation and bromide as the anion. Pyridinium modified with ethyl alcohol side chain also proves to be biodegradable with a variety of anions.[69] The biodegradability of ILs could make ILs-based materials biodegradable, thereby minimizing the impact on the environment and meeting the growing demands for materials sustainability.

ILs with biological properties of biocompatibility, anti-bacterial, and biodegradability provide another choice for researchers to develop biomaterials that have the request for biocompatibility, anti-bacterial, and biodegradability. Ionogels based on these ILs can inherit these biological properties and present potential applications in biomedical fields, for example, wearable strain sensors, drug delivery or wound healing.

3. Design strategies and fabrication methods of ionogels

Ionogels are generally designed through the formation of polymer networks in an IL medium and the IL molecules are confined in the network after gelation. Depending on formation methods, ionogels can be divided into chemically and physically cross-linked networks. Chemically cross-linked networks are constructed from covalent bonds formed by chemical reactions or polymerizations. On the other hand, non-covalent interactions, such as ionic interactions, hydrogen bonding, van der Waals interaction, host–guest interaction, *etc.*, are applied to generate physically cross-linked ionogels. RTILs, which are in a liquid state at room temperature, are usually utilized to prepare ionogels.[118] When ILs in solid state at room temperature are selected for fabrication of ionogels, they are usually used together with RTILs.[119] In this section, the preparation of ionogels using various gelators for chemical and physical gelation methods as well as their processing methods to fabricate films, foams, scaffolds, and composites will be introduced.

3.1 Ionogels using polymers as host networks

For an ideal ionogel, ILs need to be embedded tightly in a matrix structure to prevent potential loss or leaching of ILs. Polymers are extensively used as gelators to form ionogels due to their versatile skeleton design and high IL encapsulation ability.[21,120,121] The simplest method to prepare ionogels is the direct mixing of an IL with a polymer network, and ionogels can be obtained after the swelled polymer network forms a network that confines ILs. However, the miscibility of ILs with commercially available polymers, such as poly(methyl methacrylate) (PMMA), poly(vinyl alcohol) (PVA), poly(ethylene oxide) (PEO) and poly(vinylidene fluoride) (PVDF), causes preparation limitation and sometimes low IL content in ionogels.[22]

In situ gelation using monomers or polymers in the presence of an IL is an efficient strategy to form ionogels with high IL content. Free radical polymerization, ring opening polymerization, thermal and UV-curing are common techniques to form polymer networks to encapsulate ILs and yield ionogels.[122–125] These chemically cross-linked ionogels generally exhibit high mechanical strength and thermal stability, finding applications in energy and electronics materials.[13,22,126–128] Self-assembly of ABA triblock copolymers in an IL is also employed to prepare physically cross-linked ionogels.[129] The ABA triblock copolymers, such as poly (phenethyl methacrylate)-*b*-poly (benzyl methacrylate)-*b*-poly(phenethyl methacrylate) and

polystyrene-*b*-poly(diallyldimethylammonium)-*b*-polystyrene, are used as effective polymer gelators to give ionogels.[130,131] Hashimoto *et al.*[132] used polystyrene-*b*-poly(methyl methacrylate)-*b*-polystyrene (PSt-*b*-PMMA-*b*-PSt) triblock copolymers to form a physically cross-linked ionogel containing $[C_2MIM]^+[NTf_2]^-$ *via* polymer self-assembly. Aside from block copolymers, semi-crystalline homopolymers with crystalline domains can also be physically cross-linked to produce ionogels.[133]

Biopolymers such as chitosan, cellulose, starch and gelatin have also been studied as excellent gelators for ionogels.[134–137] For example, in the preparation of physically cross-linked cellulose-based ionogels, cellulose is first dissolved in an IL. Then, the cellulose-IL mixture performs gelation to form the cellulose-based ionogel due to non-covalent interactions, such as hydrogen bonds and van der Waals forces. Villar-Chavero *et al.*[136] reported the preparation of chitosan-reinforced cellulosic ionogels. The ionogels with 1 wt% chitosan loading exhibited excellent elastic moduli as 552 kPa, loss moduli as 99 kPa and complex viscosity as 22 kPa s. The selection of proper ILs and cellulose derivatives is the key to obtaining ionogels as the gelation mechanism is dependent on the IL, the cellulose structure and the cellulose concentration. In general, there are three types of chemical cross-linking methods for biopolymer-IL interactions: (i) cross-linking of functional groups, such as –OH, –COOH and $–NH_2$ with functional cross-linking reagents, such as aldehydes and carboxylic acids, *via* covalent bonds, (ii) gamma, X-ray or e-beam radiation to alter the polymers using free radicals, and (iii) polymerization.[135]

3.2 Ionogels using small molecules as host networks

The use of small-molecule gelators is another common method to prepare physically cross-linked ionogels. In contrast to polymers, small molecules here refer to organic molecules with low molecular weight, for example, dipeptides, glycolipid, 2-hydroxystearic acid and *etc.*[138] To prepare such ionogels, small-molecule gelators are added into ILs at elevated temperatures and followed by cooling to induce physical gelation through a supramolecular bonding such as hydrogen bonding, π–π interactions or electrostatic interactions. A low content ($\leq$1 wt%) of small-molecule gelators is required to form ionogels, and therefore the IL content of the ionogels could be up to 99 wt%. The high IL content and low cross-linking density of ionogels are advantageous for excellent ionic conductivity although their mechanical strengths are relatively poor. These ionogels are especially applicable for flexible electronics and stimuli-responsive materials.[139–141]

After the first example of small-molecule-gelated ionogel was reported in 2001,[142] small-molecule-gelated ionogels have gained great interest in the past two decades. For example, Wu *et al.*[143] reported a small-molecule supramolecular ionogel based on host–guest interactions between β-cyclodextrins and a bis(trifluoromethyl-sulfonyl)imide-containing IL in the presence of ethylammonium nitrate. Chen and co-workers[144] synthesized a D-gluconic acetal-based gelator which can fully mix with an IL during heating and gelation to yield an ionogel at room temperature *via* hydrophilic and hydrophobic interactions. The ionogels were injectable and exhibited high viscoelasticity, sufficient mechanical strength and self-healing behaviors. Santic *et al.*[145] reported a supramolecular ionogel using amide derivatives (*S*,*S*)-bis(eucenol)oxalamide as the gelator for $[BMIM]^+[BF_4]^-$ with a minimum gelator concentration as low as 0.7 wt%. The self-aggregation and subsequent gelation were attributed to the hydrogen bonding between the oxamides.

3.3 Ionogels using inorganic matrices as host networks

Apart from using organic matrices, ILs can also be encapsulated by using metallic or inorganic nanomaterials, such as non-metallic oxide (*e.g.*, silica), carbon nanotubes and metallic oxide (*e.g.*, titanium dioxide), to prepare inorganic ionogels. On one hand, ionogels with inorganic matrices can be prepared by dispersion of nanoparticles in an IL, followed by physical crosslinking or by sol–gel reactions. The former route can be simply achieved by the addition of the nanoparticles into an IL, and the nanoparticles can be stably suspended in the IL in the absence of surfactants or polymeric gelators.[146] The size and size distribution of nanoparticles as well as the physicochemical properties of ionic liquids are key factors to affect the formation and stability of physically crosslinked inorganic ionogels. On the other hand, the sol–gel method normally consists of sol preparation, gelation and solvent removal processes to form covalent bonds between IL molecules and nanoparticles. The first synthesis of inorganic ''dry'' silica ionogel *via* a sol–gel process was reported in 2005 following a route used by Dai and Sharp.[146–148] Dai and co-workers[146] prepared the formation of a SiO_2-based ionogel after a sol–gel reaction of tetramethoxysilane and formic acid in $[EtMeIM]^+[TFSI]^-$ (Fig. 5a). Thiemann *et al.*[149] also synthesized silane-based ionogels by using an ionic liquid ($[(EtO)_3Si\text{-}PMIM]^+[TFSI]^-$), tetramethylorthosilane and formic acid *via* a sol–gel reaction (Fig. 5b). The obtained ionogel was enabled to perform spray-coating for conductive film preparation, and the ionogel films exhibited low modulus, solution processability and high specific capacitance for flexible electronics applications. The synthesis of inorganic ionogels *via* sol–gel methods has been extensively used for electrolyte and energy materials, which are summarized in other reviews.[10,118,150] It is worth here to point out that benefit of an inorganic interface as well as the mechanical behavior of polymer could be combined as host matrices, resulting in efficient ionogels.[151]

The properties of inorganic ionogels are dependent on the size, shape, surface area and dispersion ability of the inorganic particles as well as the matrix structures of ionogels.[152] For example, Wang *et al.*[153] synthesized two silica inorganic ionogels forming by weak intermolecular forces (*i.e.*, physical crosslinking) and covalent interactions (*i.e.*, sol–gel approach), respectively. Both ionogels exhibited similar ion mobility and high long-term stability at high temperatures, while the sol–gel-generated ionogel demonstrated higher overall capacitance and electrode/electrolyte contact area. In a separate wearable device investigation, the degree of crosslinking on poly(ethylene glycol) phenyl ether acrylate networks was controlled by

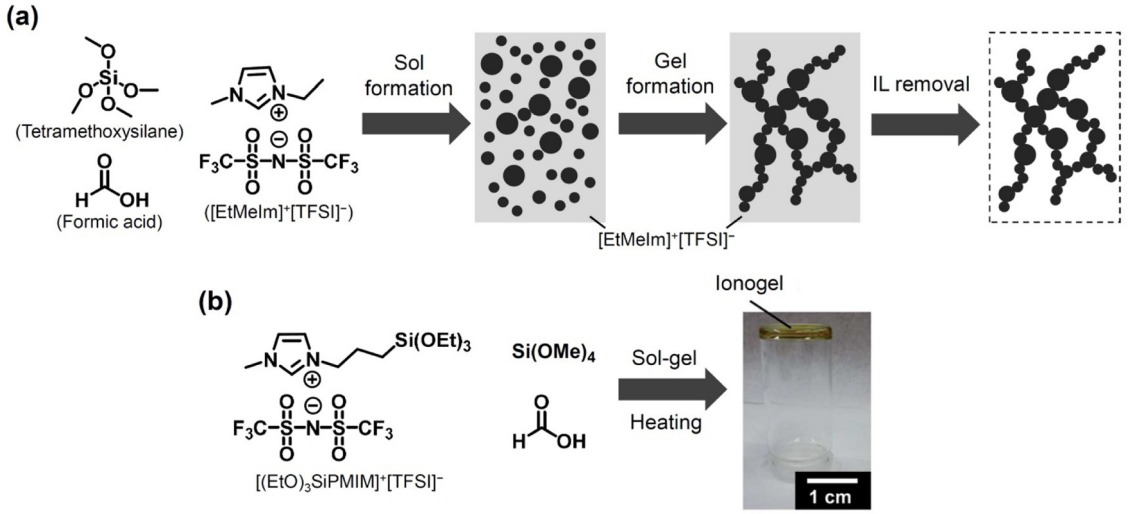

Fig. 5 Examples of ionogel preparation through sol–gel reactions. (a) Scheme of sol–gel processes. Reproduced with permission from ref. 146. Copyright 2000, Royal Society of Chemistry. (b) Molecular structures of gel precursors and $[(EtO)_3SiPMIM]^+[TFSI]^-$ ionic liquid and the image of the obtained ionogel. Reproduced with permission from ref. 149 Copyright 2014, Royal Society of Chemistry.

manipulating the silica nanoparticle dispersion for ionogel preparation.[154] These photonic ionogels with different gel contents were prepared by varying the duration of immersion in the polymer solutions, showing varied IL content, thermal and mechanical properties.

3.4 Ionogels by poly(ionic liquid)s

Poly(ionic liquid)s (PILs) refer to a class of ionic polymers with monomer repeating units containing IL species in the side chain or in the backbone. PILs exhibit intrinsic properties of both ILs and polymers and exhibit superior mechanical strength, durability, processability and structural versatility to ILs. Fig. 6a demonstrates the examples of cationic, anionic and zwitterionic PILs, bearing cations, anions or both on their polymer backbone. Through the combination of cations (*e.g.*, alkylammonium, alkylphosphonium, imidazolium and triazolium) and anions (*e.g.*, halides, carboxylate, nitrate, sulfonate and polyatomic inorganics (BF_4^-, PF_6^-, $AuCl_4^-$, *etc.*)) as well as various polymer structures (*e.g.*, homopolymers and copolymers), a myriad of PILs have been reported and found extensive applications in energy, catalysis, environmental and biomedical fields.[155–157]

There are two strategies to prepare PILs: (1) direct polymerization of IL monomers and (2) post-polymerization functionalization of non-ionic polymers. Polymerization techniques, including free radical polymerization, reversible deactivation radical polymerization, ring opening metathesis polymerization, step-growth polymerization, and so forth, have been used to prepare homo- and co-polymers of PILs.[156] In comparison with the other ionogels using conventional cross-linked polymers, PIL-based ionogels exhibit high compatibility with ILs to prevent phase separation. Copolymerization of IL monomers and a cross-linker in an ionic liquid as a reaction medium is reported to prepare PIL-based ionogels in many cases.[158–162] The cross-linkers could be non-ionic di-(meth)acrylates or ionic liquids with multiple polymerizable moieties, as shown in Fig. 6b. In 2005, Nakajima and Ohno reported the first example to copolymerize an IL monomer and an IL-containing cross-linker in an ionic liquid medium *via* free radical polymerization.[159] Free IL molecules were trapped *in situ* during polymerization to form a PIL-based ionogel. Chung's group[160] also used a butylimidazolium-containing IL, an IL monomer and an IL cross-linker to prepare a PIL-based ionogel for CO_2 separation from glue gas. Zhou and co-workers[162] reported a hierarchical PIL-based ionogel film, with high ionic conductivity and mechanical strength for lithium and sodium ion batteries. The ionogel film was prepared *via in situ* polymerization of an IL cross-linker (3, $X = Tf_2N$, $n = 2$) with an IL in $[EMIM]^+[TFSI]^-$. Kammakakam *et al.*[158] prepared a dual anionic–cationic ionogel composite membrane *via* photopolymerization. An IL monomer was blended with a free IL and polyethylene glycol diacrylate (PEGDA) cross-linker, followed by UV irradiation to yield flexible free-standing PIL ionogel membranes (Fig. 6c).

3.5. Processing methods of ionogels

Since the vapor pressure of ILs is known to be extremely low, the IL-containing ionogels are usually very stable and susceptible to desiccation. As a result, ionogels can be processed using a wide range of processing techniques.[22] In this section, we will highlight some common processing approaches for ionogels, from simplistic to more advanced processing methods (Fig. 7).

Typically, conventional processing approaches for solution-processable ionogels fabrication include solvent casting,[163,170–175] molding,[164,176,177] spin/blade coating,[165,178,179] ink jet printing,[180] *etc.* Steffen and co-workers[163] have prepared the antibiofouling ionogels composed of poly(vinylidene fluoride-*co*-hexafluoropropylene) (PVDF-HFP) and ILs mixture of $[C_{18}C_1IM]^+[NTf_2]^-$ and $[C_6C_1IM]^+[NTf_2]^-$ from the solution casting approach. Similarly, the conductive supramolecular ionogels with linear amphiphilic

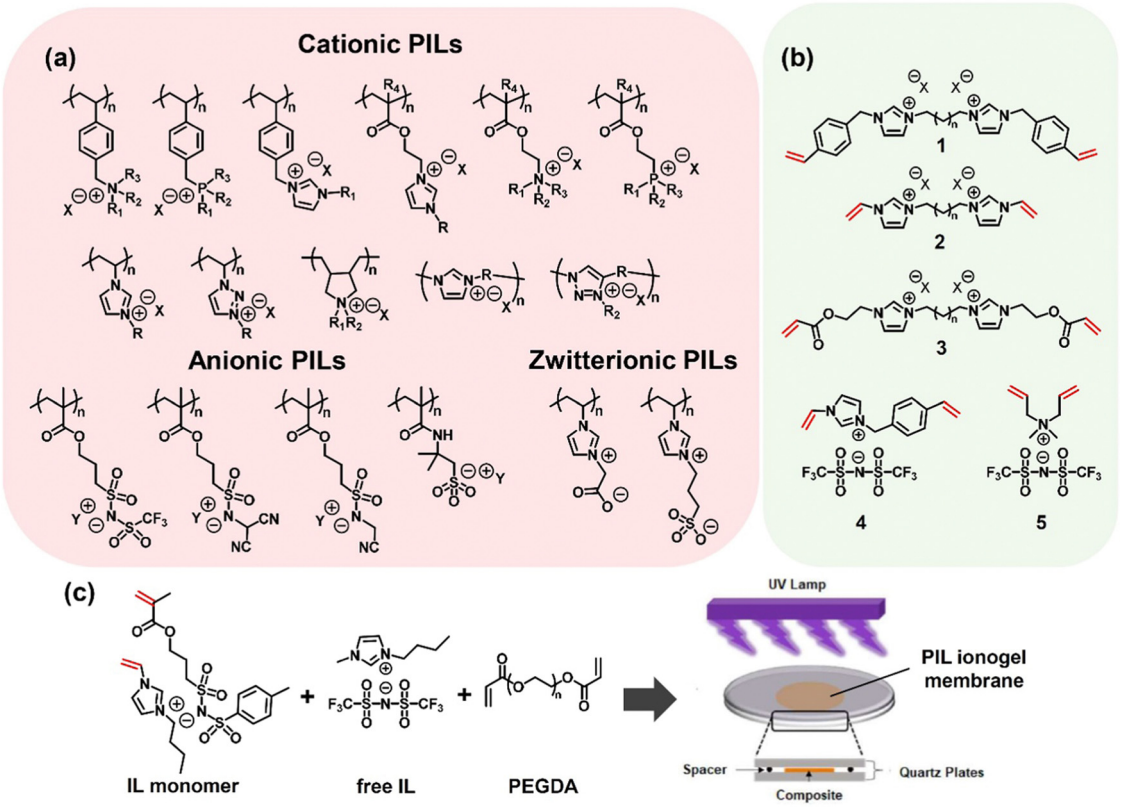

Fig. 6 (a) Examples of the chemical structure of cationic, anionic and zwitterionic PILs. (R, R_1, R_2 and R_3 = alkyl or phenyl; R_4 = H or methyl). (b) Examples of the chemical structure of IL cross-linkers. (c) Illustration of PIL ionogel membrane preparation *via* photo-polymerization. Adapted from ref. 158 with permission from American Chemical Society, Copyright 2020.

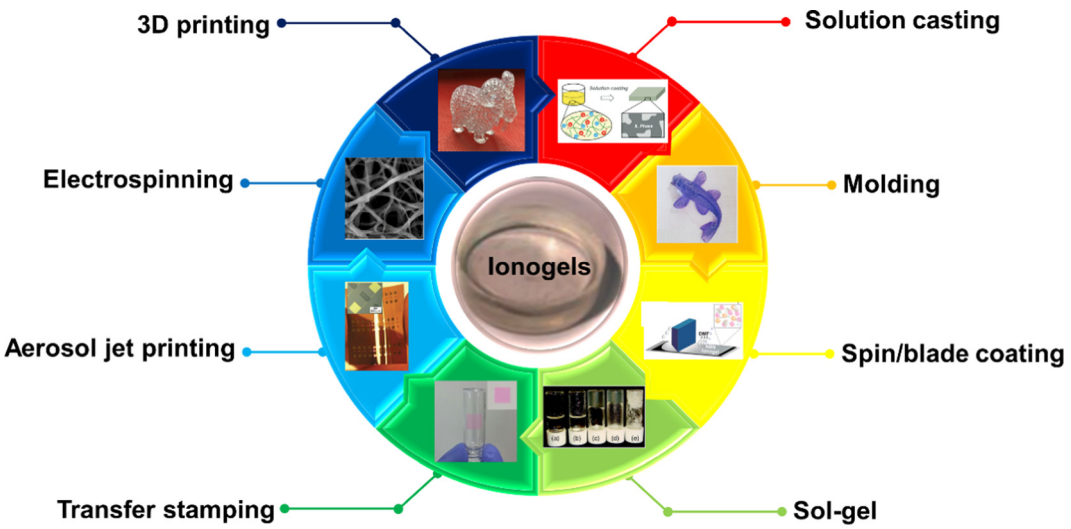

Fig. 7 Typical processing methods for ionogels. Adapted with permission from ref. 21 Copyright 2011, Royal Society of Chemistry; ref. 163 Copyright 2019, John Wiley & Sons, Inc; ref. 164 Copyright 2019, AAAS; ref. 165 Copyright 2022, American Chemical Society; ref. 166 Copyright 2010, Elsevier; ref. 167 Copyright 2017, American Chemical Society; ref. 168 Copyright 2008, Nature Publishing Group; ref. 169 Copyright 2021, American Chemical Society; and ref. 28 Copyright 2022, Elsevier.

poly(urethane–urea) (PUU) copolymer and IL $[EMIM]^+[DCA]^-$ can be easily fabricated by solution casting methods.[181]

To further obtain controlled shapes of the ionogels, solution-based molding techniques are developed. For instance, Yan *et al.*[164] demonstrated the molding capability of an ionogel prepared by click gelation of PEGDA, pentaerythritol tetra-acrylate (PETA), poly(1-butyl-3-vinyl imidazolium fluoborate), benzene tetracarboxylic acid (BTCA), triethylamine (TEA) and

1,2-ethanedithiol (ED), and then soaking IL 1-propyl-3-methylimidazolium fluoborate at 80 °C under vacuum. As the click gelation process was completed in the solution form with the methanol solvent, the click-ionogels can be molded into multiple shapes of circles, butterflies, leaves, and fish. Moreover, ionogels composed of PVA/poly(vinylpyrrolidone) (PVP) polymeric complex and IL $[EMIM]^+[DCA]^-$ were fabricated by Sun's team by casting the aqueous solution into the Teflon or silicone mold with different shapes, which fulfilled the requirements of the particular design structure of ionogels for application.[176] Other PVDF-based ionogels using the DMF route were also used for casting onto complex electrode structures.[182,183]

The spin coating method is another common approach to preparing ionogels thin films designed for small-scale microdevices. Noh *et al.*[179] reported polyurethane ionogels with IL $[EMIM]^+[TFSI]^-$ in dimethylformamide (DMF) which was spin-coated into thin films for the organic transistor and pressure sensor assembly. Besides, blade coating techniques are also developed as an effective approach for ionogels fabrication. Hersam and co-workers[165] developed an ionogel composed of hexagonal boron nitride (hBN), $[EMIM]^+[FSI]^-$ and LiFSI salt with DMF as the solvent. The final hBN ionogel slurry exhibited good capability to be blade-coated with tunable viscosity, which provided a route for the scalable production of electrochemical devices.

Sol–gel techniques are usually used to form porous ionogels.[147,166,184–188] The conventional sol–gel method involves the liquid phase removal from the gel with the remaining inorganic oxides containing porous xerogels or aerogels. As for ionogels fabrication, due to the nonvolatility of the IL, it will be incorporated within the porous solid network, which leads to the physical properties combination of the solid network and IL in resulted ionogels.[188] The confined IL filled in the interconnected porous networks still exhibits liquid-like dynamics, sometimes enhanced thanks to interfacial effects,[14] and thus give rise to the ionic conduction. Through this sol–gel route, the ionogels could be easily shaped without further processing, in the absence of chemical reactivity between the components.[166] Other ionogel synthesis routes will have to be chosen if there is any non-desired chemical reaction. Besides, the functional solutes can be included in the ionogels during the sol–gel process owing to the high solvation power of the IL. These properties enable ionogels by sol–gel methods in a wide range of applications.

Transfer stamping techniques have been used to deposit various organic and inorganic materials onto target substrates with high yield and accuracy. Studies have shown the viability of transfer stamping methods using ionogels, with tunable shapes, sizes or thicknesses, which is advantageous to apply ionogels in various electrochemical devices. Lee's team developed an ionogel composed of semicrystalline copolymer PVDF-HFP and IL $[EMIM]^+[TFSI]^-$ which was first solution-casted on flexible PDMS donor stamp substrates. The ionogel was then transfer stamped onto various acceptor substrates such as aluminum, polyimide, poly(ethylene terephthalate), and glass.[167,189,190] Besides, Benito-Lopez *et al.*[191] demonstrated a microfluidic paper-based analytical device (μPAD) fabricated by transfer stamping ionogels made from poly(N-isopropylacrylamide-*co*-*N*,*N*′-methylene-bis-acrylamide) polymer gels and ILs ($[EMIM]^+[ES]^-$ or $[P_{66614}]^+[DCA]^-$) from PDMS stamps to filter paper. With the aid of the transfer stamping technique, the ionogels could be easily formed to the desired Y-shape for applications.

As ionogels are solution processable, they are also compatible with high-throughput patterning methods such as printing with suitable "ink" viscosity.[192–194] Schubert *et al.*[192] investigated the ink-jet printability of the PEG-DMA ionogels with various ILs. However, to include a wide range of "ink" viscosity, aerosol jet printing of ionogels appears to be more feasible than inkjet printing.[168] For example, Lodge, Frisbie and co-workers[194] developed an ionogel ink combining ABA triblock poly(ε-decalactone)-*b*-poly(DL-lactide)-*b*-poly(ε-decalactone) and ILs ($[P_{14}]^+[TFSI]^-$) which was aerojet printable towards organic transistor devices.

Electrospinning has been widely applied to a wide range of materials from inorganic to polymeric materials to design nanofibrous membranes for wearable electronic devices for permeability, flexibility, and comfortability. Taubert has discussed the electrospinning techniques applied to ionogels and the progress made several years ago.[195] Applications such as catalysis, energy storage, water treatment, biomedical applications, *etc.* have been reported for electrospun ionogel membranes. More recent studies on electrospun ionogels focus more on sensing, health monitoring and motion monitoring field. Chen and Zhu *et al.*[169] demonstrated that thermoplastic polyurethane (TPU)/$[EMIM]^+[NTf_2]^-$ ionogel solution was electrospun into nanofibrous mats. The reported strain/temperature sensing performance was further enhanced attributed to the designed 3-dimensional (3D) network architectures of the nanofibrous sensors. Besides, Han and co-workers[196] fabricated TPU/IL ionogel mats using two-step fabrication processes, which combined the electrospinning of host polymer TPU and IL saturation to the electrospun polymer mats. However, the electrospinning of ionogels still has its own drawbacks, such as the limitation in capable host polymer for electrospinning and the low overall throughput over processing times.

Unlike conventional processing methods, 3D printing has the potential to fabricate precise 3D structures with a more simplified preparation process and product diversification. Moreover, most of the reported ionogels fabricated with other solution processing methods are often limited to 2-dimensional (2D) structure construction. Therefore, 3D printing technology as an emerging strategy for building sophisticated architectures has been focused on for ionogels fabrication recently. One common route is direct-ink-writing (DIW) using ionogel solutions.[181,197–199] Guo *et al.*[181] demonstrated that PUU copolymer/$[EMIM]^+[DCA]^-$ ionogel dissolved in methanol were easily 3D printed into designed patterns, such as spider webs, mesh films and cuboid specimens. Tome *et al.*[198] recently reported a biocompatible PVA-tannic acid-cholinium lactate (PVA-TA-$[Ch]^+[Lac]^-$) ionogel which also showed the capability to be directly 3D-printed. As for the UV-curable ionogels, stereolithography (SLA) and digital light printing (DLP) are suitable for more sophisticated 3D architecture fabrication.[28,200,201] Furukawa *et al.*[202] successfully developed an

ionogel composed of $[BMIM]^+[FSI]^-$ and UV-induced crosslinking of a thiol-ene network which was suitable for SLA-based 3D printing. The ionogels could be printed into various shapes, sizes and complexity at the highest resolution of 200 μm from the pre-gel solution with rapid UV curing. Song *et al.*[200] very recently reported stretchable ionogels with multiple networks of IL 3-dimethyl (methacryloyloxyethyl) ammonium propane sulfonate (DMAPS) and acrylic acid in $[EMIM]^+[EtSO_4]^-$, with acrylate-terminated hyperbranched polyester polyols (HP, with eight double bonds and eight hydroxyls) as chemical macro-cross-linkers. The reported highest resolution of ionogel printing *via* DLP techniques can reach ~10 μm, which was much higher than the most commonly used extrusion-based 3D printing technique for ionogels. Furthermore, Nelson and co-workers[203] prepared a mechanochromic ionogel by DIW printing, which utilized a single mechanoactivation event to elicit both mechanochromic response and autonomous shape change (mechanomorphic) in the object. This technique was also recognized as 4D printing.

4. Materials characteristics of ionogels

Ionogels retain many distinct characteristics from intrinsic ILs and gelators, such as mechanical strength and viscoelastic behaviors, excellent ionic conductivity, great thermal and electrochemical stability and non-volatility.[11,22,120] In this section, some typical properties and emerging properties of ionogels will be highlighted, as well as how they enable ionogels to be used in a variety of applications (Fig. 8).

4.1 Rheological and mechanical properties

The mechanical and rheological properties of ionogels are one of the crucial parameters depending on the application. So far, most of the ionogels possess weak mechanical properties, such as low tensile strength, fracture toughness and tensile modulus.[164,210–212] As a consequence, ionogels find mass application in the fields such as wearable electronics, sensors and actuators.[213] Efforts have been made to tune the mechanical properties of the ionogels for better usage performance on the basis of understanding of key factors that influence the rheological and mechanical properties of ionogels.[211,214,215] In general, the rheological and mechanical properties of ionogels are strongly related to the characteristics of the ionogel host networks, such as cross-link density. For instance, an ionogel composed of poly(ethyl acrylate)-based elastomers and $[NTf_2]^-$-based ILs were reported by Liu *et al.*,[211] which exhibited high and tunable mechanical properties by varying the cross-link density of the ethyl acrylate (EA) and ethylene glycol dimethacrylate (EGDMA) network. With the increase of cross-link density from 0.34 to 2.72, Young's modulus of the ionogel was enhanced from 15 to 484 kPa, while the strain at fracture noticeably decreased from 490 to 80%. At a cross-link density of 0.68, the elastic modulus of the ionogels with 23 wt% IL content was reported at 250 kPa and a record-high fracture toughness of 4.7 kJ m^{-2} was achieved. Moreover, a fluorinated acrylic double-network (DN) ionogel was reported by Qiu *et al.*[214] by chemically cross-linking methyl acrylate (MA) and 2,2,3,4,4,4-hexafluorobutyl acrylate (HFBA) with cross-linker EGDMA and curing the swollen poly(methyl acrylate-*co*-2,2,3,4,4,4-hexafluorobutyl acrylate) P(MA-*co*-HFBA) single (1st) network infused with monomers and cross-linkers. With fixed IL $[EMIM]^+[TFSI]^-$ content and cross-link density of the second network, it was found that a slight increase in fracture strength and Young's modulus when increasing the cross-link density of the first network by adding more EGDMA cross-linkers from 0.5% to

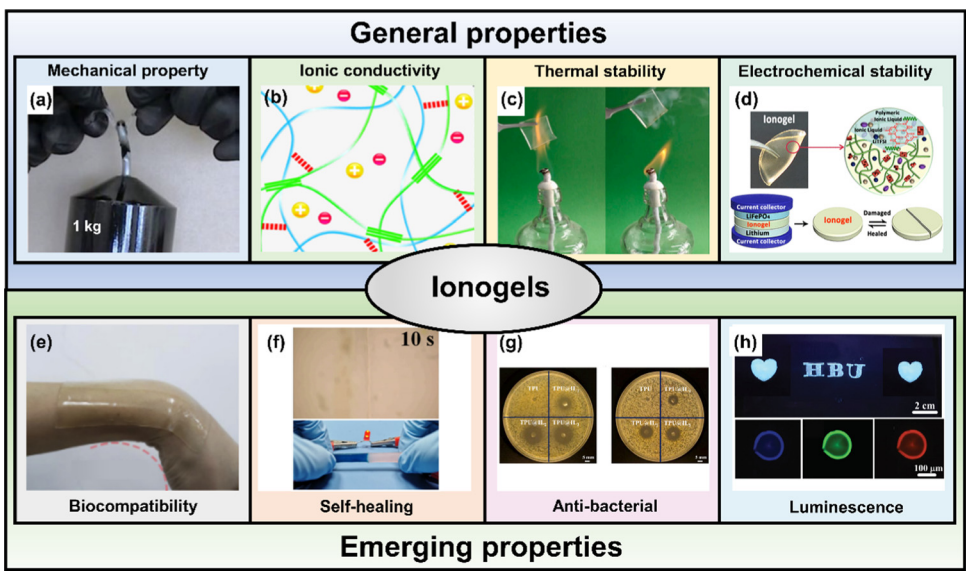

Fig. 8 Schematic illustration of the unique ionogels properties. Reproduced with permission from (a) ref. 204. Copyright 2022, Nature Publishing Group; (b) ref. 176. Copyright 2020, American Chemical Society; (c) ref. 205. Copyright 2022, Elsevier; (d) ref. 206. Copyright 2019, American Chemical Society; (e) ref. 207. Copyright 2020, Cell Press; (f) ref. 208. Copyright 2021, American Chemical Society; (g) ref. 24. Copyright 2021, Elsevier; (h) ref. 209. Copyright 2021, Royal Society of Chemistry.

1%, while the elongation of break and toughness decreased. A similar phenomenon has also been found with physically cross-linked ionogels. As an example, Xia *et al.*[216] reported that a physically cross-linked ionogel consisting of poly(*N*,*N*-dimethylacrylamide) (PDMAA), $[CMMIM]^+[TFSI]^-$, and metal–organic frameworks (MOF) (UiO-66 and HKUST-1) coordinates with polymer chains. This designed coordination between metal sites of MOF and PDMAA polymer chains induced reversible physical cross-links and hindered the formation of covalent cross-links in the polymer matrix. With the increase of MOF loading, the cross-link density of the ionogel increased and the fracture strength was enhanced with sacrifice in elongation at break.

In addition, the characteristics of ILs play a significant role in the mechanical properties of ionogels. ILs can act as plasticizers when used as the dispersing medium during the preparation of ionogels.[199,217] Due to the strong hydrogen bonding and electrostatic interactions, the weakening in interactions between polymer chains and lowering the polymer crystallization thus leads to enhanced ionogel stretchability but decreased Young's modulus. For example, Shi and co-workers[218] reported an ultra-stretchable semicrystalline fluorinated copolymer ionogel with ILs $[BMIM]^+[TFSI]^-$. The plasticizing effect of $[BMIM]^+[TFSI]^-$ to the copolymer lowered the glass transition temperature (T_g), which contributed to the enhanced stretchability (>6000%) of the ionogels. Tamete *et al.*[219] studied the effect of IL chemical structure on viscoelastic characteristics of ionogels where they attribute the influence to the hydrogen bonding between IL anions, cations and polymer gelators. When hydrogen bonding is weak for ILs, the strong hydrogen bonding between copolymer micelles resulted in phase separation and hence fragile ionogels.

The mechanical properties of ionogels could also be tuned over a wide range by simply varying the IL contents or the polymer and inorganic content.[151] Wu *et al.*[29] reported facile one-step polymerized $[DMAEA\text{-}Q]^+[TFSI]^-$ ionogels in $[N_{4111}]^+[TFSI]^-$. The mechanical properties of the ionogels were tailorable by changing the molar percent concentration of IL $[N_{4111}]^+[TFSI]^-$. With the increase of ILs from 5% to 35%, Young's modulus and strain at break were modulated in the range of 337 to 0.22 MPa and 349 to >10 000%, which was due to the plasticizing effect of $[N_{4111}]^+[TFSI]^-$. The ionogels also exhibited excellent adhesion ability with the highest adhesion strength of 38.73 ± 7.5 kPa to porcine skin of 25% IL loading, which was higher than the commercial gel electrodes. Furthermore, to withstand the harsh environmental conditions for specific applications such as ionogel electrolytes between the anodes and cathodes in lithium-ion batteries, highly robust ionogels with over 10 MPa were developed.[10,120,220] Phase separation caused by the polymer gelators in ILs plays an important role in the mechanical property of ionogels. Huge progress was recently made by Hu and Dickey *et al.*[204] that they reported a polypol(acrylamide-*co*-acrylic acid) (P(AAm-*co*-AA)) ionogel in $[EMIM]^+[ES]^-$. Copolymerization of acrylamide and acrylic acid in $[EMIM]^+[ES]^-$ resulted in a macroscopically homogeneous covalent network with *in situ* phase separation, where the polymer-rich phase with hydrogen bonds dissipated energy and toughened the ionogel, while the elastic solvent-rich phase enabled large strains. The copolymer ionogels showed record-high mechanical properties of fracture strength (12.6 MPa), fracture toughness ($\sim$24 000 J m^{-2}) and Young's modulus (46.5 MPa). The ionogels also exhibited high stretchability ($\sim$600% strain), good self-recovery, shape-memory and self-healing properties.

4.2 Ionic conductivity

Ionic conductivity is a key feature of ionogels, which are inherited from ILs. Unlike the low ionic conductivity ($\sim 10^{-2}$ S m^{-1}) of PILs with ILs as structural units due to restricted ionic transport after polymerization,[221,222] the ionogels composed of free ILs and polymeric or inorganic host networks exhibit relatively high ionic conductivity as the cations and anions move freely as a mobile phase.[21,223] Generally, the ionic conductivity of ionogels is affected by multiple parameters. First, the chemical structures of ILs largely influence the ionic conductivity of the ionogels. Ionogels consisting of anions with weak hydrogen bonding capabilities such as $[BF_4]^-$, $[PF_6]^-$ and $[DCA]^-$ usually exhibit better ionic conductivity.[224] Besides, other natures of ILs such as viscosity and ion sizes also play crucial roles in the ionic conductivity of ionogels. It has been reported that the longer alkyl chain of cationic counterparts causes higher viscosity and reduced cation mobility, which lowers the ionic conductivity of ionogels. Therefore, to improve the ionic conductivity of ionogels, ILs with low viscosity and smaller ion sizes are preferred. For instance, Liu *et al.*[225] reported bacterial cellulose-based ionogels with the integration of imidazolium-based ILs. Ionogels with 95 wt% of $[EMIM]^+[BF_4]^-$ exhibited a high ionic conductivity of 3.41×10^{-2} S cm^{-1}, which is higher than that of 95 wt% $[EMIM]^+[NTf_2]^-$. The difference in ionic conductivity with identical IL loading was ascribed to the viscosity and ion size difference, where $[EMIM]^+[BF_4]^-$ possessed a lower viscosity and smaller anion size than $[NTf_2]^-$. Furthermore, proper selection of pore size and volume in ionogel cross-link networks also contributes to enhanced ionic conductivity. Ding *et al.*[226] found that by tuning the concentration of poly-(2-acrylamido-2-methyl-1-propanesulfonic acid) (PAMPS) in the ionogel cross-linked network, micropores increased and the enlarged specific surface area and pore volume led to better absorption of ILs, thus ionic conductivity was enhanced from 0.6 to 1.7 S m^{-1}. Moreover, studies also found that the crystallinity and T_g also influence the ionogel conductivity. Weng and co-workers[176] did investigation on the $[EMIM]^+[DCA]^-$/polymer composite ionogels with different ratios of PVA and PVP. The ionic conductivity of the composite ionogel was found to be enhanced with higher PVP loading, as the PVP integration led to the decrease in crystallized PVA and the increased free volume in composite ionogels facilitates the IL movement. The ionic conductivity of ionogels can also be simply tuned by adjusting the composition of the ILs and the gelators in the ionogels. Increasing the content of ILs in ionogels enhances the ionic conductivity closing to the value of neat ILs,[227] while the mechanical properties may suffer losses. For instance, an

increasing trend in ionic conductivity of the PUU/$[EMIM]^+[DCA]^-$ ionogel from 0.072 S m^{-1} to 2.25 S m^{-1} was reported by Chen *et al.*[181] as the loading of IL concentration increased from 20 wt% to 60 wt%. Moreover, experiment results evidenced that the temperature increase will also lead to ionic conductivity increase owing to the better flexibility of the polymer chain and higher ion mobility under higher temperatures. As an example, Lan *et al.*[228] reported the dependence of ionic conductivity of the poly(methyl methacrylate-*co*-butyl methacrylate)(P(MMA-*co*-BMA))/$[EMIM]^+[TFSI]^-$ DN ionogel. The ionic conductivity of the ionogel increased by over 250-fold with a temperature increasing from −40 °C to 80 °C owing to the increased flexibility of polymer chains and the increased ion motility of ILs.

4.3 Thermal stability

The thermal stability of ionogels is another crucial parameter that enables ionogel-based devices to be operated in a high temperature range. TGA is commonly used for evaluating the thermal stability or degradation behavior of ionogels. As discussed in the previous section, ILs possess excellent thermal stability with T_{onset} over 250 °C. Therefore, the IL-containing ionogels also exhibit excellent temperature resistance. Variously reported ionogels are thermally stable at a high temperature range of over 200 °C.[200,201,205,229–232] For instance, Hu *et al.*[232] reported that the P(MMA-*co*-BMA 2-hydroxyethyl acrylate) (PHEA) ionogel possessed excellent thermal stability as it started to decompose at 250 °C, while the employed ILs $[C_2MIM]^+[EtSO_4]^-$ possessed decomposition temperature of 330 °C. Furthermore, Liu and co-workers[211] reported that the poly (ethyl acrylate)/$[C_2MIM]^+[NTf_2]^-$ ionogels with EGDMA cross-linking agent exhibited excellent thermal stability up to 330 °C in an N_2 atmosphere, with only 2% of weight loss. Studies have shown that the thermal stability of ILs can be enhanced by tuning IL structures such as alkyl chain length, alkyl substituents and functional groups, thereby improving the thermal stability of ionogels.[233] The thermal stability of gelators also plays an important part that affecting the thermal stability of ionogels. Inorganic nanoparticles are widely acknowledged for excellent thermal stability. Therefore, composite ionogels formed from inorganic nanoparticles (such as SiO_2, TiO_2) exhibit excellent thermal stability, even though a slight decrease in thermal stability is found after ILs confined in these highly thermally resistive matrices.[10,234,235] For instance, the SiO_2-IL-TFSI ionogels prepared by Lu *et al.*[236,237] exhibited exceptional thermal stability where the hybrid ionogel is thermally stable up to 400 °C. Typically, inorganic nanoparticle ionogels prepared using the sol–gel approach usually exhibited deteriorated thermal stability due to the by-products during the synthesis process.[238] TGA results showed that the T_{onset} of the SiO_2-based ionogel using the sol–gel approach is lower than the ionogels prepared by direct mixing of fused silica and ILs, where the difference was attributed to the by-products during the chemical reactions.[153] It also has to be pointed out here that the liquid range of confined ILs is also extended towards low temperatures, below solidification temperatures of non-confined ILs, thus extending the temperature range of applications.[239] ILs thus can improve the anti-freezing ability of ionogels under sub-zero temperatures. Xu *et al.*[240] reported an anti-freezing ionogel with T_g as low as −55.9 °C based on the IL and the poly(urethane) (PU) matrix. The PU ionogel showed excellent stability in a −20 °C environment for 10 days, where the sensing performance remained the same as a fresh ionogel. Another ionogel reported by Ren *et al.*[231] exhibited thermal stability over an exceptionally wide temperature range from −108 to 300 °C. The ionogel can withstand freeze-heating cycles and showed stable storage and loss moduli between −105 and 250 °C and long-term thermal stability at 250 °C for 5 days.

4.4 Electrochemical stability

Due to the large electrochemical stability window (ESW) of ILs, the ionogels composed of such ILs typically exhibit high electrochemical stability which are suitable for electrochemical applications such as ionogel electrolytes.[10,206,241–244] The electrochemical stability significantly affects the cycle life of ionogels, and it is determined by the oxidation potential and reduction potential. Generally, piperidinium and pyrrolidinium-based ILs usually exhibit higher oxidation potentials than imidazolium-based ILs but lower ionic conductivity.[224,245] For instance, solid-state ionogel electrolyte prepared by confining IL $[Py_{13}]^+[TFSI]^-$ and $[Li]^+[TFSI]^-$ within sol–gel prepared TiO_2 gelators exhibited high electrochemical stability with the anodic limiting potential reaching about 5 V *versus* Li/Li^+.[246] Another work done by Guo *et al.*[206] demonstrated the ionogel membranes consisting of hydrogen-bonded supramolecular PIL-UPy copolymer networks and $[DEIM]^+[TFSI]^-$. The ionogel membrane exhibited a wide electrochemical stability window up to ~5 V *versus* Li/Li^+. Wu and Lu *et al.*[243] reported a SiO_2 nanoparticle incorporated ionogel electrolyte with ILs $[BMIM]^+[TFSI]^-$ and $[Li]^+[TFSI]^-$ with enhanced anodic stability (5.2 V *vs.* Li/Li^+), where the enhanced anodic electrochemical stability was attributed to the presence of SiO_2 nanoparticles. More strategies have been reported to further improve the electrochemical stability of ionogels, such as modification of surface interactions between the ILs and matrices. Hersam *et al.*[244] found that the hBN nanoplatelet solid matrix of the hBN/$[EMIM]^+[TFSI]^-$/$[Li]^+[TFSI]^-$ ionogel improved anodic electrochemical stability to 5.3 V *versus* Li/Li^+ comparing to that of the IL electrolyte alone (4.2 V *versus* Li/Li^+). Moreover, compared to the bulk hBN, the exfoliated hBN showed more suppression on the decomposition peak owing to the larger surface area to stabilize Li-based ILs.

4.5 Emerging properties and functions

In addition to the above-mentioned properties of ionogels, with the variance of the ILs, polymer networks and added functional fillers, the resulting ionogels could possess diverse interesting functional properties, such as biocompatibility,[194,198,247] biodegradabilities,[135,194,248,249] self-healing properties,[208,250–252] shape-memory,[253] luminescence properties[186,200,209,254,255] and antibacterial properties.[24,256,257] These distinct properties endow ionogels with a wide range of applications.

Biocompatibility is a crucial property for biomedical-related ionogels, particularly for bioelectronics application that needs to be adhered to the skin or implanted in the body. Generally, biocompatible ionogels are prepared from Bio-ILs, whose anionic and cationic counterparts are usually derived from natural or biocompatible substances,[67] such as amino acids,[106] glucose,[258] and *etc.* Recently, cholinium has emerged as the most common cationic moiety in the structure of biocompatible ILs.[74,198,259–261] To obtain the fully biocompatible ionogels, biocompatible gelators are usually used, such as PVA,[198] cellulose,[261,262] poly(ε-caprolactone) (PCL)[194] and *etc.* For instance, Mecerreyes, Minari, Tome and co-workers[198] reported a biocompatible cholinium-based ionogel with PVA and plant-derived polyphenol compounds (PhCs). The ionogels were formed by hydrogen bonding dynamic crosslinking between biocompatible PVA and gallic acid, tannic acid and pyrogallol in the cholinium based ILs $[Ch]^+[Ac]^-$ and $[Ch]^+[Lac]^-$. Besides, low toxicity ILs can also be used to prepare biocompatible ionogels. Frisbie and Lodge *et al.*[194] designed biocompatible ionogels with low toxic $[P_{14}]^+[TFSI]^-$. The biocompatible triblock copolymer consisting of poly(DL-lactide) and PCL formed self-assembled micellar cross-links in $[P_{14}]^+[TFSI]^-$ similar to thermoplastic elastomers. The results provided abundant candidates for both the constituent ions of ILs and monomers of aliphatic polyesters that opened a large variety of possible combinations for biocompatible ionogels. In addition to the ILs/polymer ionogels, biocompatible PILs were also reported by Mecerreyes *et al.*247 In this work, a series of cholinium-based methacrylic ILs were photopolymerized into biocompatible ionogels.

Biodegradability is another emerging property for ionogels recently because of the increasing demands in materials sustainability to minimize the environmental impact. Even though studies have been reported on ILs biodegradation,[109,263] limited work has been done on biodegradable ionogels. Most of the reported biodegradable ionogels focus on using biodegradable materials as network matrices. Examples vary from biopolymers (such as cellulose and its derivatives,[135,170,225,262] gelatin[137]) and biodegradable copolymers.[194,248] For example, Migliorini *et al.*[249] developed an ionogel consisting of nature-derived biodegradable 2-hydroxyethyl cellulose and $[Ch]^+[Lac]^-$. With the aid of the spray casting technique, the fabricated biodegradable supercapacitor with ionogel electrolyte showed great eco-friendliness. Zhang and co-workers[248] recently developed an ionogel by using $[EMIM]^+[BF_4]^-$ and biodegradable polyurethane made from poly(L-lactide) (PLLA), poly(D-lactide) (PDLA), and poly(ethylene glycol) (PEG) as a scaffold. The stereocomplex nanocrystallite (sc) PLA-PEG ionogels exhibited biodegradability, ascribing to the presence of biodegradable polyurethane.

Ionogels can also exhibit self-healing behaviors, which mostly arise from the hydrogen bonding and coulombic interactions between gelators and ILs. Numerous efforts have been applied to explore the self-healing properties of ionogels for various applications. For example, Li *et al.*[250] reported a ZnO reinforced poly(acrylic acid) (PAA)/$[EMIM]^+[OAc]^-$ ionogel which exhibited decent self-healing behavior with high mechanical strength. Xu and Dong *et al.*[252] developed a multifunctional ionogel based on Ag-Lignin nanoparticles, NCO-ended polyurethane, and ILs ($[EMIM]^+[DCA]^-$). The fabricated ionogels were able to self-heal from scratch after heating at 50 °C for 1 h with the best healing efficiency of 97.6%. Moreover, Zhang, Liu and co-workers[208] reported ultrafast self-healable ionogels based on PVA-polyacrylamide (PAAm)-choline chloride ($[Ch]^+[Cl]^-$)/ethylene glycol. The ionogel demonstrated an extremely fast self-healing performance of crack disappearance in 10 seconds under 25 °C. The shape memory ability is another emerging property of ionogels as it may be applied to flexible actuators and pressure sensors. Recently, Liu and Zhao *et al.*[253] reported shape and stiffness memory ionogels which were made from ILs and uniformly dispersed poly(stearyl methacrylate) (PSMA) micro-inclusions. By combining the microstructure alignment for stiffness changing and shape memory micro-inclusions for stiffness fixing, the hetero-phase ionogels exhibited tunable compressibility, which could be fabricated into pressure sensors with programmable performance.

The anti-bacterial property of ionogels originates from the nature of ILs. The electrostatic interaction between ILs cationic groups and the bacterial cell could lead to the deactivation of the cell membrane. Furthermore, the hydrophobic alkyl chains of ILs could also be inserted into cell membranes, causing the death of bacteria. As an example, Zhu *et al.*[24] reported ionogels by mixing polyurethane and $[EMIM]^+[NTf_2]^-$, which could serve as temperature and strain sensors. The introduction of ILs into polyurethane endowed the ionogels with significant anti-bacterial function towards both *E. coli* and *S. aureus*. The anti-bacterial effect was found to increase with the IL contents increasing. In contrast, no anti-bacterial effect was observed for pure polyurethane, confirming the antibacterial effect of ionogels originating from ILs. Kumar *et al.*[264] fabricated an ionogel film by the hydrogen bonding between gelatin and choline salicylate. The ionogel films showed excellent anti-bacterial activity against *Bacillus subtilis* owing to the presence of IL choline salicylate, showing great potential for applications in food packaging.

Typical luminescent inorganic or organic dyes can be incorporated into the ionogels to form luminescent ionogels. Earlier studies by Binnemans *et al.*[254] reported that by doping the europium(III) tetrakis β-diketonate and lanthanide(III) complexes into $[C_6MIM]^+[NTf_2]^-/SiO_2$ networks, the resulting ionogels revealed very strong photoluminescence with different colors under ultraviolet light irradiation, moreover with luminescence decay times as long in ionogels as is non-confined ILs thus highlighting the beneficial effect of liquid dynamics of confined ILs. Later, Taubert *et al.*[265] reported luminescent PMMA ionogels containing $[BMIM]^+[NTf_2]^-$ and a/d-block chromophores based on platinum and europium. The as-fabricated ionogel showed bright red luminescence typical of europium(III) upon ultraviolet irradiation at 365 nm. Recently, Song's team developed a novel strategy to fabricate photoluminescent ionogels without any conventional conjugated chromophores, rare earth ions, or quantum dots.[200,209] The ionogel exhibited special

aggregation-induced emission (AIE) properties, attributed to molecular motion restriction by special cross-linking structures. Therefore, the photoluminescent ionogels emitted light of blue, azure blue, and green to red at various irradiation excitation wavelengths from 365 nm to 550 nm.

5. Biomedical applications of ionogels

In recent years, the use of gel-based biomedical materials becomes more attractive. Ionogels which possess advantages of good ionic conductivity, flexibility, and thermal stability as well as the properties of anti-bacterial and biocompatibility have emerged as promising candidates for biomedical applications. In this section, various applications of ionogels in biomedical fields such as wearable and sensing applications (for human motion detection, health monitoring, human–machine interface), therapeutic delivery systems, wound healing and biochemical detection will be introduced.

5.1 Wearable and sensing applications

In biomedical applications, due to the thermal stability, ionic conductivity, electrochemical stability inherited from ILs, tunable mechanical properties of flexibility, stretchability, and durability, as well as the emerging properties of biocompatibility, self-healing ability, ionogel-based wearable sensors are gaining popularity and traction.[176,209,218,266,267] Most of the present ILs used for ionogel-based wearable sensors are aprotic ILs. When selecting ILs to prepare ionogels for wearable strain sensors, the interactions between ILs and gelators should also be considered. So far, many ionogel-based wearable sensors have been demonstrated which can respond to various environmental stimuli, including pressure, strain, deformation, humidity and temperature, transmitting signals to wearable sensing applications such as motion detection, healthcare monitoring, and human–machine interface.[268,269] In this section, we will discuss the details of these ionogel-based wearable sensing devices and briefly highlight the current progress.

5.1.1 Human motion detection. Human motion detection becomes the key for various intelligent wearable devices applying these materials to perform like our natural skin (Young's modulus of 0.14–0.60 MPa) in different body motions.[269] Motions that mimic human activities in large body motions, such as the movement of the finger, wrist, elbow, neck, or knee bending/unbending at various angles, fist clenching-unclenching, as well as complex and delicate small muscle motions, such as speaking (vocalization and pronunciation), swallowing, and pulse detection.[270] In some reports, dynamic motion of the lower body (jumping, walking, and running) and neck movement (turning, nodding, and shaking) is also demonstrated.[24,28,217] In addition, the adhesion performance of the developed strain sensor to the different substrates such as metal, plastic, glass, rubber, paper, and wood is vital for maximum contact between the sensor and the human skin.[269,271] This intimate contact allows precise body movement recognition essentially translated to high sensitivity and response. The sensitivity of the strain sensors is evaluated by the higher gauge factor (GF), which is the relative change in electrical resistance ($\Delta R/R_0$) as a function of the mechanical strain (ε).[177]

In one work, Sun and Li developed ultra-durable ionic skins (I-skins) with excellent self-healing ability and broad sensitivity to strain (1–300%) and pressure (0.1–20 kPa).[268] The PU network is composed of dynamically crosslinked crystallized PCL and flexible PEG with hindered urea bonds (HUB) and hydrogen bonds, followed by impregnation of ILs composed of $[DEIM]^+[TFSI]^-$. Due to the high electrochemical stability of the IL, there was no hysteresis in the relative change in electrical resistance ($\Delta R/R_0$) as a function of low strains of 0–50% and large strains of 50–300%, showing excellent motion sensing capability. The I-skin showed great response over multiple pulse measurements obtained by fixing the I-skin on the wrist and repeated bending/unbending movements of the finger and the elbow. In addition to static movement demonstration, Xu *et al.*[217] also presented dynamic motion like running, walking, and jumping, and small muscle sensitivity in pulse detection and several pronunciations, as illustrated in Fig. 9. The team developed physically crosslinked ionogels based on 2,2,2-trifluoro ethyl acrylate (TFEA) and the acrylamide copolymer polymer network and a hydrophobic ionic liquid, $[EMIM]^+[TFSI]^-$. The resultant ionogel has abundant fluorine that enables excellent water and solvent resistance, and the non-covalent interactions, such as ion–dipole and hydrogen bonding, yield excellent strength and resilience. The developed ionogel showed high transparency, self-healing, and self-adhesive properties in air and underwater, excellent solvent tolerance, and low-temperature tolerance. In another work, Lan and Shi fabricated high transparency (>93%) dual-network (DN) ionogels made by physically cross-linked PVDF-HFP and chemically cross-linked P(MMA-*co*-BMA) elastomer networks within $[EMIM]^+[TFSI]^-$ ionic liquid.[228] PVDF was selected due to its good mechanical properties, thermal stability, and electroactivity, while P(MMA-*co*-BMA) was selected due to elastomeric properties and its outstanding IL compatibility. The developed DN ionogel contained a high content of 70% IL and possessed good mechanical performance (failure tensile stress 2.31 MPa, strain 307%) and strain sensitivity (GF = 1.62) for various body motions. The highly durable ionogel strain sensors showed a fast response, wide sensing range and sensitive detection to different motions at various degrees and multiple cycles, including finger, wrist and elbow. The flexible strain sensors were also capable of sensing slight throat jitter during swallowing and vocalization at the neck region. Notably, the dual-network ionogel also shows great response under extreme temperature conditions (−40 to 80 °C). Recently, Xu and Zhu designed a bioinspired interlocked hexagonal microcolumn array structure using laser-etched silicon wafers *via* the template transfer approach.[272] In their design, $[EMIM]^+[NTf_2]^-$ and TPU were selected as the conductive component and polymer matrix due to good compatibility and interfacial interaction, respectively. The IL/thermoplastic polyurethane (TPU@IL) ionogel exhibited pressure-sensing

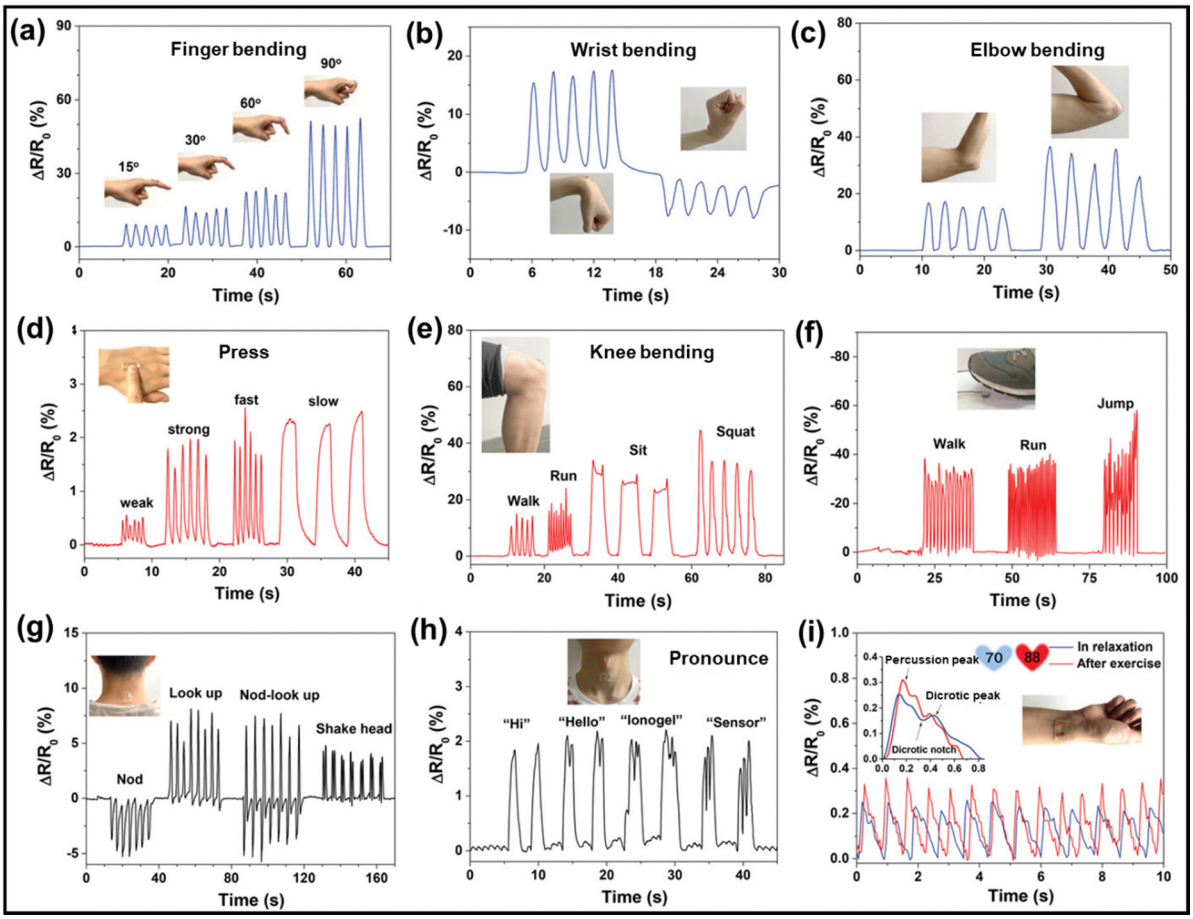

Fig. 9 Real-time monitoring of human motions and subtle physiological signals by ionogel-based sensors. Signals of relative electrical resistance during (a) finger bending, (b) wrist bending, (c) elbow bending, (d) press, (e) knee bending, (f) walking, running, and jumping, and (g) neck movements. Relative resistance variations during (h) speaking different words and (i) radial pulse of the wrist at ease and after exercise. Inset: Variations of wrist pulse patterns with an unnoticeable tidal wave at ease (blue) and a high tidal peak after R_1-exercise (red). Permission from ref. 217 Copyright 2021, John Wiley & Sons, Inc.

properties, which had an ultralow detection limit (~10 Pa) and ultrafast responsiveness (~24 ms), attributed to the interlocked microstructure, like the epidermal–dermal layers of human skin. Likewise, ionogels also exhibited excellent skin adhesion and motion sensitivity. The team demonstrated responsiveness to the press and release of the finger, bending the knuckle, and feeble pressure from the weight of the rice grain. Respiration detection through breathing and pulse reading was also demonstrated. They further demonstrated the potential of the ionogel sensor in information encryption and distress signals transmission by pressing the sensor with variable pressing time using the principle of the International Morse Code. In another recent work by Feng and Liu, they employed a thermo-spun reaction encapsulation strategy and developed knittable fibrous ionic conductors with a wide temperature tolerance, high fatigue resistance, and wearing comfort.[266] The team demonstrated a core-sheath structure based on the hydrogen-bonded poly (ionic liquid)-backboned ionogel (HB-PILI), $[EMIM]^+[DCA]^-$ as the ionic conductive core and thermoplastic elastomer (TPE) as the highly elastic sheath. Due to the strong interfacial interaction between the IL and polymer matrix, the resulting fiber exhibits low hysteresis, high conductivity (44 mS cm^{-1}), wide detecting capability, and remarkable sensitivity. Additionally, the comfortable fibrous and stretchable ionic sensors could adhere well to human skin, have excellent cyclability (5000 cycles) and exhibit excellent real-time monitoring of large and facet joints movement based on the finger, wrist, elbow, and knee.

5.1.2 Health monitoring. Another key application is real-time health monitoring and assessment, where the wearable strain sensor can precisely detect physiological signals and monitor pulse, eye movement, and breathing (deep or shallow) patterns.[273] These real-time examinations of patients' physiotherapy and health conditions during any form of physical activity play a significant role in a patient's motor function restoration.[274] For instance, Mecerreyes and co-workers[259] reported photopolymerized poly(cholinium lactate methacrylate)-based ionogels with biocompatible and low toxic IL $[Ch]^+[Lac]^-$. The excellent compatibility between poly (cholinium lactate methacrylate) and $[Ch]^+[Lac]^-$ prevented ILs from a major concern of leaching when attached to the skin. After adding free ILs to 60 wt%, a decrease in T_g to −70 °C was

obtained from −40 °C of the homopolymer poly(cholinium lactate methacrylate), giving the ionogel excellent flexibility and softness for wearable applications. The ionogel is then designed to use as the solid electrolytic interface between skin and electrodes, and the electrocardiography (ECG) signals were recorded with ionogel assisted electrodes for up to 3 days. A biodegradable cholinium-based ionogel with polycarbonate gelators prepared by ring-opening polymerization of cyclic carbonate monomers in imidazolium lactate ILs showed the capability to take up 10–30 wt% of ILs and became softer materials by increasing the amount of free ILs.[275] The ionogels exhibited similar impedance decrease with the human skin to levels of commercial Ag/AgCl electrodes, which showed excellent capability in a cutaneous electrophysiological recording. Most recently, 3D-printed sensors for ECG recording were fabricated from biocompatible PVA-tannic acid-cholinium lactate (PVA-TA-$[Ch]^+[Lac]^-$) ionogels.[198] Selected ionogels were incorporated onto Kapton and textile electrodes and then used as the electrolytic interface between the electrodes and the skin, which displayed similar performance of ECG recordings compared to medical standard electrodes. The ECG monitoring in different environment such as underwater conditions during diving was further realized with the development of water-resistant ionogels reported by Wu *et al.* (Fig. 10A).[29] The ionogel consisted of C–F bond-rich hydrophobic polymer networks which endowed the ionogel with excellent stability, adhesion and self-healing properties underwater. The ionogel electrodes demonstrated good efficiency in collecting real-time ECG signals both in air and underwater, which was essential for health monitoring during sports and daily life.

In addition, the breathing signals could also be detected by ionogel-based wearable sensors *via* humidity changes.[276,277] For example, Wang *et al.*[276] fabricated chemoresistive humidity sensors based on SiO_2/IL hybrid ionogels which could realize real-time human breath monitoring by impedance change with changing humidity. The fastest response and recovery time of the $SiO_2/[BMIM]^+[Br]^-$-based sensors reached 3 s and 10 s, respectively. The improved sensitivity characteristics of $SiO_2/[BMIM]^+[Br]^-$ could be attributed to its high conductivity and hydrophilicity, leading to fast ion transfer using $[Br]^-$ and $[H_3O]^+$ as charge carriers under humid conditions. Moreover, in another recent work, Chen and Zhu *et al.*[169] electrospun a fibrous mat with aligned nanofibers of TPU@IL ionogels that possessed good breathability desired for wearable electronics in addition to the good mechanical performance and excellent temperature-sensing behaviors. The excellent strain and temperature sensing capabilities in various simulated testing, as shown in Fig. 10B, facilitated precise detection of respiration and proximity. Furthermore, the ionogel sensor could be connected to the wireless transmission device to remotely monitor human motion and physiology, which is a value-adding feature as demonstrated in many studies.[240,278]

5.1.3 Human–machine interface. Another critical application of wearable sensors is the human–machine interface (HMI), where sensors capture the real-time hand motion and convert it into a digital signal, followed by real-time wireless transfer to the resultant devices, such as a mechanical hand that recognizes hand gestures, a highly controllable drone[279] or an Unmanned Aerial Vehicle (UAV).[280] These developments demonstrate huge potential in virtual reality interaction and motion control in the future. In an earlier work by Amoli and Kim, they created a bio-inspired ionic mechanoreceptor skin, a synthetic multicellular hybrid ion pump composed of silica microstructures (artificial mechanoreceptor cells) embedded

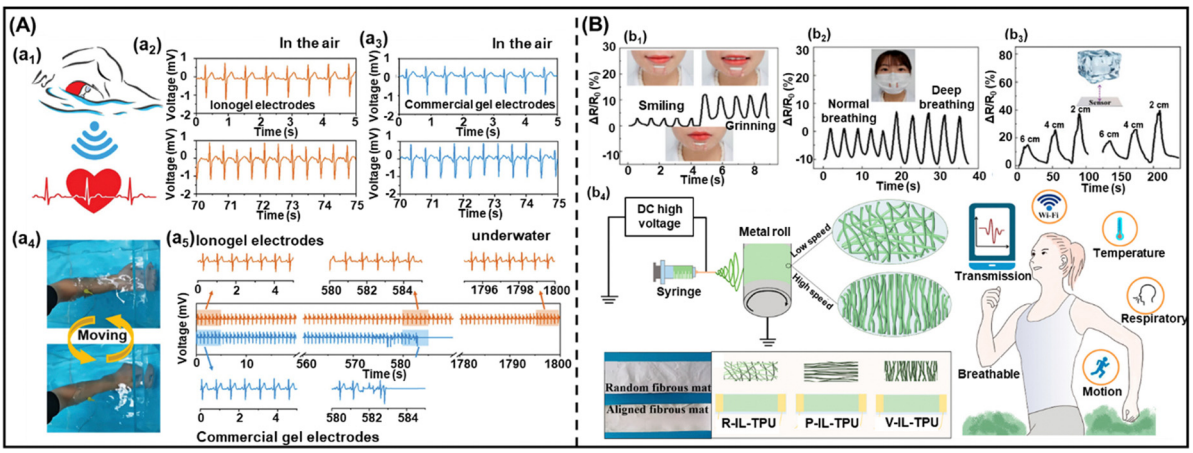

Fig. 10 (A) Schematic illustration of a biocompatible PVA-tannic acid-cholinium lactate (PVA-TA-$[Ch]^+[Lac]^-$) ionogel for ECG recording in the air and underwater. (a_1) Schematic diagram of ECG signals detected by the ionogel electrode underwater; (a_2) ECG signals recorded by an ionogel electrode when a volunteer is at rest (top) and running (bottom); (a_3) ECG signals recorded by CGE while the volunteer was resting (top) and running (bottom); (a_4) photos of ECG signals detected by the ionogel electrode during human movement underwater; (a_5) long-term stability of ECG signal detected by CGE and ionogel electrode in the aquatic environment. Reproduced with permission from ref. 29. Copyright 2021, John Wiley & Sons, Inc. (B) Schematic demonstration of the V-IL/TPU ionogel sensor. Real-time response of the V-IL/TPU sensor to the (b_1) facial muscle, (b_2) normal breath and deep breath of a volunteer. (b_3) Dependence of the $\Delta R/R_0$ signal of the V-IL/TPU sensor on the distances between a piece of ice (inset) and the sensor. (b_4) Scheme for connecting the V-IL/TPU sensor to the wireless transmission device remotely monitoring human motion and physiology. Permission from ref. 169. Copyright 2022, American Chemical Society.

into thermoplastic polyurethane elastomeric matrix (artificial extracellular matrix) with hydrogen-bonded $[EMIM]^+[TFSI]^-$ ion pairs on the surface.[279] The group integrated and demonstrated the ultrasensitive (48.1–5.77 kPa^{-1}) ionic mechanoreceptor skin sensor array and a flexible printed circuit board (PCB) onto a wearable aerial drone microcontroller (WADM). The resultant HMI could precisely command the drone's aerial flight, including controlling the drone's height, rotation speed, and direction using the WADM, as illustrated in Fig. 11A. In another work, Wang *et al.*[280] developed a flexible, transparent, and self-healing polymerized ionogels wearable HMI utilizing a signal processing system, and self-healing strain sensor arrays. The ionogel constructed by silica and $[VEIm]^+[DCA]^-$ simultaneously provides an elastic solid frame and the IL enables electrical conduction. The strain sensor showed high sensitivity with a max GF of 20 and a wide sensitivity detection range of 0.2–3000%. The wearable HMI could effectively capture various eye movements through four-array strain sensors. Based on the coupling effect of different sensors, the wearable HMI collected and processed the signals of the four sensors under different movements of the eyes, and then output different signals to control the movement and maneuver in different directions (right, left, up and down) of the Unmanned Aerial Vehicle (UAV).

In recent work, Zhang and Song developed a 3D printable nanocomposite chemically crosslinked ionogel and demonstrated good capability in human motion detection.[28] The dual cross-linking structure ionogel was fabricated by one-step photopolymerization. The design is composed of polyhedral oligomeric silsesquioxanes (POSS) nanodots as multifunctional chemical crosslinking points and PAA hydrogen bonds as reversible physical crosslinking points, impregnated with the high ionic conductive liquid, $[EMIM]^+[(EtO)_2PO_2]^-$. In their design, $[EMIM]^+[(EtO)_2PO_2]^-$ was preferred due to the (i) great miscibility with PAA, (ii) exceptional dispersibility and stability for the POSS nanodots, and (iii) excellent solubility of POSS and PAA in the IL. The constructed high-performance ionogel displayed ultrahigh stretchability (~7000%), high conductivity, self-healing capability, self-adhesiveness, and superior wide tolerant temperatures (−78–235 °C), attributed to the strong interfacial interaction. The ionogel was subsequently translated to the wearable HMI. Remarkably, the sensor could identify and differentiate the human gestures in real-time and convert them to a digital signal and real-time wireless transfer to a mechanical hand to realize the hand gesture recognition, as illustrated in Fig. 11B. The team successfully developed a high-sensitivity robotic hand that reconstructed human finger and wrist motion accurately and seamlessly. Moreover, the excellent results were also demonstrated under a wide temperature range, from extremely low temperatures (−60 °C) to relatively high (150 °C) temperature settings, attributed to the selection of the materials. Their developed mechanical hand showed excellent anti-freezing properties and high thermal stability that enabled great versatility and employment in harsh environments, an essential

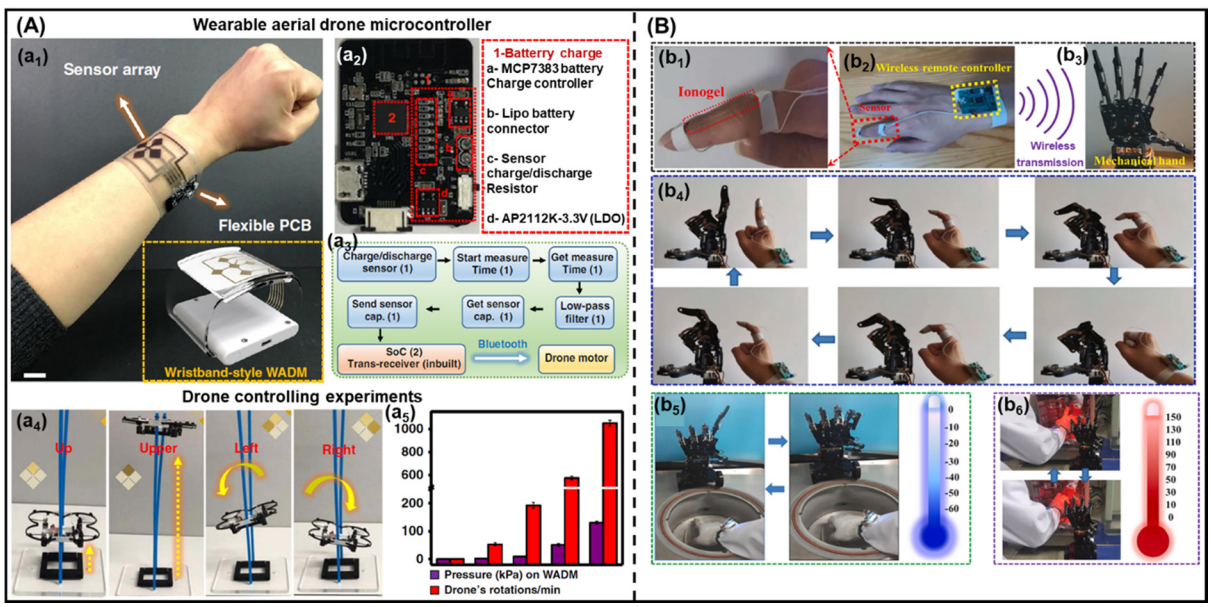

Fig. 11 (A) (a_1) Photograph of a WADM (fabricated by integrating the IL–silica–TPU flexible pressure sensor array of 4 pixels and flexible wireless PCB) attached to a wrist. Scale bar, 2 cm. (a_2) Photograph of commercially available flexible wireless PCB with different integrated circuit components labeling. (a_3) System-level functional block diagram of WADM shows different steps of signal processing and wireless transmission features enabling aerial drone control. (a_4) Photographs of real-time experiments of aerial drone control, which include controlling the drone's height, rotation speed, and direction. (a_5) Bar curve shows a qualitative response of the drone's RPM to the pressure applied on the sensor array of WADM. Permission from ref. 279. Copyright 2019, Nature Publishing Group. (B) The real-time wireless human–machine interface control system. (b_1–b_3) Schematic of the system. The response of an ionogel-based sensor from hand motion is first real-time captured and converted to the digital signal, and then the data is real-time wireless transferred to a mechanical hand. (b_4) Human hand gesture recognition and mechanical hand real-time response and reconstruction. (b_5 and b_6) Human–machine interface under −60 °C and 150 °C. Permission from ref. 28. Copyright 2022, Elsevier.

consideration for many of the reported research in other applications.[209,228,269,271]

5.1.4 Other ionogel strain sensing. Ionogel-based sensors can also be used in other emerging applications such as soft robotics and implantable biomedical devices. Soft and innovative materials based on ionogels enable soft robots or ionotronics to adapt and mimic the motions and functions of biological systems. The developed ionotronics need to possess the desired physical (mechanical, thermal) and application (ionic conductivity, sensitivity, adhesion, recyclability) performance to mimic and perform like our natural skin (Young's modulus of 0.14–0.60 MPa). The properties of ionogels offer the possibility of their applications in soft robotics or implantable biomedical devices. For instance, Sun *et al.*[281] designed a new type of triboelectric nanogenerator (TENG) based on an ionogel, known as I-TENG. The ionogel system is formed by two main interactions. First, the dipole–dipole interactions between the pendant zwitterionic functional groups on the 3-dimethyl (methacryloyloxyethyl) ammonium propane sulfonate (DMAPS) portion, and second, the ion–dipole interactions between ionic liquid ions, $[EMIM]^+[DCA]^-$ and ionized groups. The developed ionogel exhibited high transparency, deformability, durability, and stable electrical performance over a wide temperature range from −20 to 100 °C in unstretched and stretched states. The developed I-TENG had a high-efficiency biomechanical energy harvesting and self-powered physiological monitoring, showing great potential in soft robotics and intelligent soft control panel. In a similar application, Yiming *et al.*[230] fabricated an ionogel based on copolymer ethylene glycol methyl ether acrylate (MEA) and isobornyl acrylate (IBA) as the polymer network with $[C_2MIM]^+[TFSI]^-$ as the ionic conductive phase. $[C_2MIM]^+[TFSI]^-$ was chosen due to its hydrophobicity and low viscosity, contributing to low hysteresis and water resistance in the resultant ionogel. The engineered ionogel exhibited desirable conductivity (10^{-4}–10^{-5} S cm^{-1}), stretchability (>2000%), and wide temperature tolerance (−60 to 200 °C). The group demonstrated multimodal sensing abilities, including resistance, capacitance, short-circuit current, and open-circuit voltage as TENG and sensory I-skin, a potential candidate for soft ionotronics. In another study, the poly(urethane) (PU)-based ultradurable I-skins developed by Sun and Li showed great robustness and high elasticity, with Young's modulus of ∼0.42 MPa that was very similar to that of human skin.[268] The authors reported the potential for implantable devices and soft robotics.

In a recent development, Ma and Qu developed an ionogel-based multifunctional sensor consisting of a waterborne polyurethane (WPU) network with highly conductive and hydrophilic ILs, $[EMIM]^+[TFSI]^-$, and nanofillers (amino modified halloysite nanotubes (mHNTs).[270] The developed ionogel possesses good durability, high sensitivity, and multi-signal detection capability in diverse application environments. The micro nanostructured ionogel-based I-skin (MIS) had biomimetic hierarchical structures that enabled a wide sensing range of strain (0.1–400%), pressure (0.001–15 kPa), and temperature (25–95 °C). Given its hydrophilicity design, the ionogel is proficient in detecting subtle underwater vibrations caused by liquid drops or waves, a robotic fish, or human action, as illustrated in Fig. 12. This soft robotic with the developed ionogel showed diverse applications, including biological research. In a recent study by He *et al.*[282] the team designed a biology-inspired structure and conceptualized a novel fingerprint-inspired conformal buckling on a sheath-core ionogel-fluoroelastomer sensory fiber. The fluoroelastomer, PVDF-HFP-TFE [poly(vinylidene fluoride-hexafluoropropylene-tetrafluoroethylene)] terpolymer and the hydrophobic ionic liquid $[EMIM]^+[TFSI]^-$ formed the sheath and core, respectively. To further enhance the ionic conductivity and the interfacial adhesion between the fluoroelastomer sheath and the IL core, a copolymer $[PMEA\text{-}co\text{-}MTMA]^+[TFSI]^-$ ionogel was incorporated as the tie layer. The core material composed of $[PMEA\text{-}co\text{-}MTMA]^+[TFSI]^-$ ionogels and ionic liquid $[EMI]^+[TFSI]^-$ initially optimized the internal dipolar and hydrogen bonding interactions, followed by coating the fluoroelastomer sheath to reduce the environmental interference from humidity. The bioinspired buckled fiber possessed excellent stretchability (730%) and exceptional strain sensitivity (GF = 10.1) than the conventional smooth fiber, showing great inspiration in the future fiber-based ionic conductors for miniatured implantable strain sensors.

5.2 Therapeutic delivery system

The employment of gels to load drugs for mucosal delivery is an effective approach when intravenous and oral administration is not suitable, for example, if drugs tend to be eroded or broken down in the digestive system. Ionogels are just emerging as carriers for drug release. This is based on the fact that ionogels could slowly lose ILs and internal loads. A common issue with many drugs is their hydrophobic nature, which leads to low solubility in aqueous solutions. Therefore, many studies are dedicated to looking for ways to improve the solubility of drugs or other feasible measures. ILs have been demonstrated to dissolve substances that are sparingly soluble or insoluble in aqueous solutions and organic solvents.

The biologically active ILs provide the possibility for ionogels to be used in the drug release area.[103] The ionogels used for drug delivery should have good biocompatibility, usually made from Bio-ILs whose cations and anions are derived from natural or biocompatible materials, such as amino acids, glucose, and carboxylic acids. Pharmaceutical ingredients containing ILs are another candidate to fabricate the ionogels for drug delivery,[67] where ILs and drugs could complement each other. Recently, Mitragotri's group designed a novel ionogel patch using PVA and choline and geranate (CAGE),[26] which could be used for controlled and sustained release of both insulin and the ILs in the small intestine (Fig. 13). The IL of CAGE could improve the absorption of insulin and poorly soluble drugs by the small intestine. The resulting ionogels were mucoadhesive and presented desirable release profiles for oral drug delivery. The localization of ionogel patches could reduce long-term effects on the epithelium while also limiting drug loss by the uptake of epithelial cells in oral delivery. The drug loaded ionogel patches represent a novel and useful strategy to realize the oral delivery of biologics. Moreover, Shayanfar *et al.*[283] reported an ionogel system containing an

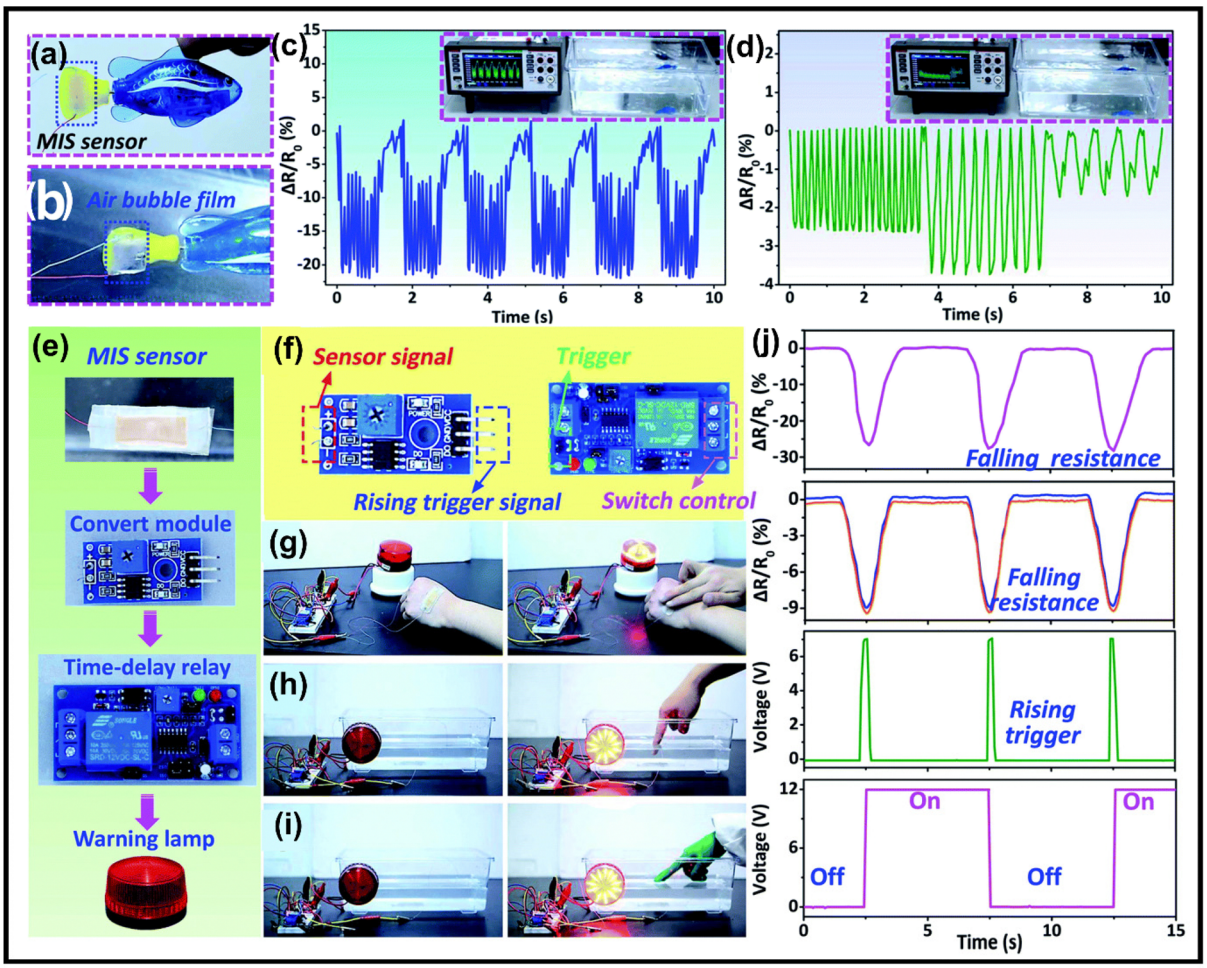

Fig. 12 (a–d) Applications of the MIS-based sensors in real-time detection of motions and subtle vibrations in an aqueous environment. (a) MIS sensor attached to the robotic "fishtail", (b) a layer of significant air bubble film forms on the MIS sensor due to its excellent superhydrophobicity. (c and d) the relative resistance variations of the MIS sensor in response to the constant and different swing frequencies of the "fishtail". (e–j) Applications of the MIS sensor in a smart warning lamp control system. (e) Photographs of the circuit of the alarm lamp control system. (f) The functions performed by the conversion module and the time delay relay during signal transmission. (g–i) Application of the alarm lamp control system in different scenarios. (j) The corresponding signal transmission and conversion process. Permission from ref. 270. Copyright 2021, Royal Society of Chemistry.

anti-cancer drug of sunitinib malate (SUM). The drug-loaded ionogels were prepared by polymerizing 2-hydroxyethyl methacrylate (HEMA) in the mixture of SUM and therapeutic choline chloride/ascorbic acid. The fabricated ionogels were biocompatible and could make a friendly environment for cells. It is found that the ionogels could stabilize the interior drugs, which did not show any degradation for up to 6 months. It is found that the drug release rate from ionogels at pH 1.2 was faster than that at pH 6.8 and pH 7.2, which could be attributed to the protonation of the amino groups on SUM, increasing the ability to partition into aqueous solutions.

Responsive ionogels are also fabricated and utilized for encapsulating drugs, where the drugs release effect could be adjusted. In this case, Malek and co-workers[284] synthesized cetylpyridinium salicylate (CetPySal), which could form temperature responsive ionogels to load the anti-cancer drug imatinib mesylate. The three-dimensional structure of the ionogels was formed by the inter-digitation of the fibers. The physical appearance of ionogels could change with temperature from opaque to transparent due to the internal supramolecular structural arrangement. The release kinetics of the loaded drugs was explored at $T = 37$ °C with different pH values and at pH = 5.0 with different temperatures. The result indicated that the higher temperature and lower pH values facilitated the release of loaded drugs.

5.3 Wound healing

Ionogels can be used as platforms for wound healing because of their anti-bacterial activity, which is inherited from the nature of ILs.[285] ILs' lipophilicity would promote their absorption on the phospholipid bilayer of the cell membrane, whereby their charged nature would allow electrostatic interactions with the cell membrane, eventually penetrating and disintegrating the cell wall, causing cell lysis.[97] In general, ILs have a broad activity spectrum, which can be observed for Gram-positive and Gram-negative bacteria as well as mycobacteria and fungi.[101]

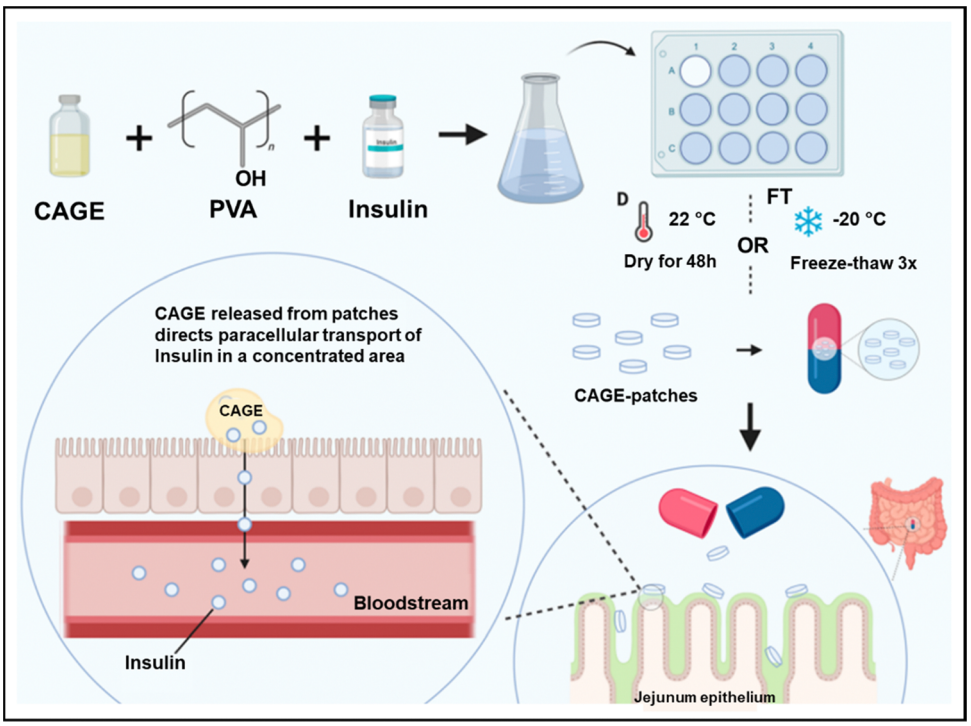

Fig. 13 Schematic representation for the fabrication of ionogel patches for drug release. Adapted from ref. 26 with permission from copyright 2020, American Chemical Society.

The antibacterial mechanisms of ILs can be ascribed to (i) cationic groups of ILs which interact with bacterial cell walls through electrostatic interaction, leading to the deactivation of membrane proteins. (ii) The hydrophobic alkyl chains of ILs which are inserted into cell membranes to disturb the membrane lipid layer structure and leak the intracellular cytoplasm, leading to the death of bacteria. ILs with long alkyl chains on the cationic groups are preferred for preparing ionogels for wound healing applications. ILs confined within ionogels reduce the potential ILs leakage for antibacterial usage, as well as can also obtain skin adhesive ability and increase the local IL concentrations.

More recently, Villar-Chavero's group[136] fabricated a chitosan-reinforced cellulosic ionogel using an ecologically safe ionic liquid of cholinium lysinate and chitosan, which was formed by hydrogen bonds. The rheological properties study indicated that with the increase of chitosan loading, the viscoelastic properties were higher, which reached the highest when the chitosan loading was 1%. The ionogels showed good anti-bacterial ability towards *S. aureus* and *E. coli.*, which presented potential applications in the pharmaceutical area. Fujita's *et al.*[286] developed a rapid and simple one-pot approach for the synthesis of transparent cellulose ionogels. They dissolved cellulose using $[C_4MPYR]^+[OH]^-$ as the solvent, after cellulose was crosslinked with epichlorohydrin (ECH): an ionogel was therefore prepared. They found that the ionogels formation time was as fast as 30 minutes and related to the crosslinker concentrations. The ionogels could swell in aqueous solutions. The water uptake, swelling ratio and mechanical strength of ionogels could be controlled by adjusting the cellulose concentration and employing water. Moreover, the cellulose ionogels here showed strong anti-bacterial activities towards *E. coli B*/*r* and *B. subtilis*, which made the ionogels as promising anti-bacterial materials for dressing wounds, especially against antibiotic-resistant strains.

Imidazolium salt based ILs are usually made into ionogels for antibacterial and wound healing applications because of the strong anti-bacterial effect. As an example, Dong and co-workers[252] prepared an ionogel based on $[EMIM]^+[DCA]^-$, polyurethane and Ag-Lignin nanoparticles (Ag-Lignin NPs). The ionogels were self-healed due to the presence of disulfide bonds and exhibited excellent mechanical properties. The catechol groups of Ag-Lignin NPs endowed the ionogels with repeatable and long-lasting adhesiveness. The obtained ionogels presented excellent anti-bacterial properties due to numerous positive imidazole ion groups and silver ions. Considering the promising applications of ionogels in wound healing, Yan's group prepared amino acid-based PIL membranes for dressing skin wounds,[287] which were infected by methicillin-resistant Staphylococcus aureus (MRSA) (Fig. 14A). The anti-bacterial effect of the PIL membranes enabled them to accelerate wound healing and alleviate tissue inflammation. They found that the PIL membranes based on ionic bonds presented higher anti-bacterial activity than those based on covalent bonds. The PIL membranes based on D-enantiomeric amino acids showed higher antibacterial activities compared with those based on L-enantiomeric amino acids. Furthermore, the fabricated ionogel membranes could alleviate tissue inflammation and accelerate the wound healing process. Mao and co-workers[288]

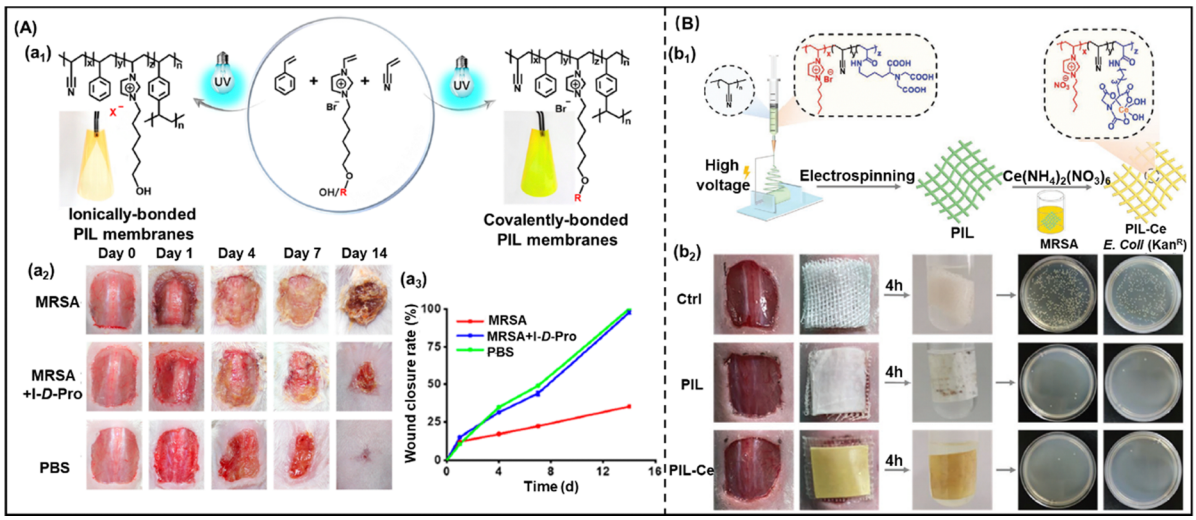

Fig. 14 (A) Schematic representation for the design of the PIL ionogel membranes and the wound-healing assessment: (a_1) illustration of the PIL membranes preparation; (a_2) representative images of MRSA-infected wound healing process; (a_3) wounds closure rate at 14 days post-operation from PBS negative controls, the PIL membrane treated mice and MRSA positive controls. Reproduced with permission from ref. 287. Copyright 2019 American Chemical Society (B) schematics of poly (ionic liquid)/Ce-based membranes (PIL-Ce) for wound treating: (b_1) illustration of the PIL membranes preparation with the ability of anti-bacterial and disintegrating antibiotic resistance genes; (b_2) images illustrating the wound treating assessment of PIL based membranes in a mouse model infected with bacteria. Reproduced with permission from ref. 288. Copyright 2021 John Wiley & Sons, Inc.

synthesized PIL/cerium(IV) based electrospun membranes (PIL-Ce) (Fig. 14B). The membrane exhibited excellent antibacterial ability and could break down drug-resistant genes. The wound healing test demonstrated that membranes with good cytocompatibility and hemocompatibility could be used for blocking the spread of drug resistance in clinical applications. Yan *et al.*[25] reported Zn-containing PILs membranes that showed antibacterial activities. The wound healing test demonstrated that the membranes were biologically safe and could accelerate wound healing.

5.4 Biochemical detection

Biochemical detection is an emerging application of ionogels in recent years. Due to the high conductivity and broad electrochemical window as well as the thermal stability inherited from the nature of ILs, ionogels are widely employed as electrochemical sensors. As an example, Silvester *et al.*[289] fabricated an electrochemical sensor for detecting 2,4,6-trinitrotoluene based on ionogel films, made from $[P_{14,6,6,6}]^+[NTf_2]^-$ and poly(hexyl methacrylate). The IL of $[P_{14,6,6,6}]^+[NTf_2]^-$ provided ionic conductivity and facilitated the preconcentration of 2,4,6-trinitrotoluene into the films. This electrochemical sensor realized the sensitive detection for 2,4,6-trinitrotoluene with a detection limit of 0.37 μg mL^{-1}. Huang *et al.*[290] prepared an electrochemical sensor for detecting rutin, on basis of the PIL/IL-graphene modified electrode.[246] Owing to the presence of ILs as good conductivity agents, the electrodes modified with ILs of carboxymethyl-3-methylimidazolium chloride showed the best electrochemical performance compared to those without ILs, thus exhibiting excellent detection ability towards rutin. Linearity from 0.03 to 1 μM for rutin analysis was obtained by the electrochemical sensor, and the limit of detection was as low as 0.01 μM. Moreover, the sensor could selectively detect rutin and be utilized for determining rutin in tablets. Valentini and co-workers[291] fabricated graphene/ILs ionogel electrodes for caffeic acid determination. $[BMIM]^+[Br]^-$ and $[BMIM]^+[Cl]^-$ were selected to prepare graphene/ILs composite ionogels because of their relatively high electrochemical conductivity, wide potential window and low viscosity. This electrochemical sensor could selectively detect caffeic acid with a fast response time (2 s) and a detection limit of 0.005 mM. Wang's group[292] developed a screen-printed electrode based on tetrathiafulvalene (TTF)-tetracyanoquinodimethane (TCNQ)/$[BMIM]^+[PF_6]^-$ ionogels for the detection of tyrosine. Ag/AgCl was selected as the reference electrode, and ionogels modified carbon served as the working electrode. Due to the high electronic conductivity and stability of the ionogels, this electrochemical sensor could selectively detect tyrosine with good stability and sensitivity.

The sensitive detection of ultralow concentrations of NOx in exhaled breath is significant for diagnosing health disorders, such as asthma, cystic fibrosis, and bronchiectasis. Following this thought, Ha's group fabricated an electrochemical gas sensor employing ionogels for detecting biomarkers in exhaled breath.[27] The ionogel was fabricated by immobilizing $[EMIM]^+[TFSI]^-$ within the PVDF-HFP polymer matrix, which was developed for NOx gas sensors on polyethylene terephthalate substrates. The thermal stability of $[EMIM]^+[TFSI]^-$ and hydrophobicity of PVDF-HFP ensured the long-term stability of the ionogel-based gas sensors. The sensing performance of the gas sensor increased as IL content increased because of sufficient ions reacting with gas molecules, then decreased abruptly as the amount of IL increased owing to the low viscosity of the ionogel. The electrochemical gas sensors presented a sensitive response towards 300 ppb of NOx target gas for 15 s of exhaled

breath duration. In addition, Silvester and co-workers[293] fabricated $[C_2MIM]^+[NTf_2]^-$/PILs membranes on planar electrode devices for electrochemical gas sensing. The mixture of ILs and PILs endowed the membranes with adequate conductivity and robustness for gas determination. These membranes were mechanically stable and reproducible current responses, which could be utilized for O_2, NH_3, and SO_2 sensors. Gruber's group fabricated an electronic nose based on ionogels,[294] which served as the sensitive layers for detecting volatiles. After absorbing and dissolving volatiles, the viscosity of ionogels changed, leading to an increase in conductance. This could realize the detection of volatiles. The fast-response electronic nose could distinguish different volatiles with an accuracy above 98%.

6. Conclusion and future perspective

In recent years, ionogels, as soft materials composed of ionic liquids confined within various matrices, have aroused more and more attention. The preparation, properties and processing methods of ionogels are introduced here. We then focus on the emerging biomedical applications in this review. The properties and biomedical applications of ionogels are related much to the ILs species and the processing methods. Due to the ionic conductivity, non-flammability, thermal stability and wide electrochemical window, ionogels present promising applications in wearable strain sensors and electrochemical detection. The cations endow the ionogels with excellent antibacterial performance and wound healing. Drug release is based on the fact that ionogels could slowly lose ILs and internal loads. The ionogels based on biodegradable ILs also facilitate the applications in drug release.

The main existing challenges of ionogels for biomedical applications are mainly how to balance the cost and performance, how to develop more biocompatible ILs and design clever structures. In addition, ILs have a high affinity with water, leading to additional efforts to be dried, which may in turn increase the cost of final products. A Lot of ILs are neither biocompatible nor biodegradable, which limits the further applications of ionogels in the human body but well chosen, ILs are human-body compatible. For the drug release and wound healing applications, in addition to concern about the biocompatibility of ILs, we should also pay enough attention to preparing more intelligent ionogel systems, for example, stimuli-responsive drug release systems. The biodegradability of ionogels should also be concerned. The complete degradability of ionogels should include the degradability of both ILs and host networks. However, currently, quite limited data are available on fully biodegradable ionogels. The present reports of biodegradable ionogels mainly focus on the use of biodegradable polymers as the matrix, rare attention is paid to the simultaneous degradation of ILs and the matrix. A feasible way to fabricate fully biodegradable ionogels is to select ILs with biodegradability discussed in Section 2.2, and biodegradable polymers as gelators, for instance, poly(lactide), poly(hydroxybutyrate) or nature-derived biopolymers. In short, it is better to select high conductivity, cheap, degradable, and biologically safe ILs to prepare ionogels for biomedical applications. In addition, complicated synthetic processes should also be avoided.

The future exploration of biomedical applications of ionogels are mainly (i) to develop new ionogels by customizing cations and anions meeting specific applications in the biomedical area; (ii) through rational design, reducing the toxicity of imidazolium-based ionogels, or developing other more biocompatible ionogels for potential human body applications; (iii) to fabricate stimuli-responsive ionogels for potential drug release applications, for example, fabricating magnetic-responsive ionogels employing magnetic ILs; (iv) to build the recycling procedures for ionogels, decreasing the negative impact to environments and save costs.

In conclusion, this review offers a comprehensive perspective on the recent progress of ionogels for biomedical applications ranging from wearable strain sensors to biochemical detection. Considering the numerous ILs types and various host networks, ionogels with new properties and biomedical applications are expected to continue to emerge in coming years, this research area is still in its infancy. We believe that ionogels for biomedical applications will be commercially available in the near future.

Abbreviations

$[TFSI]^-$	Bis(trifluoromethyls-ulfonyl)imide
$[NO_3]^-$	Nitrates
$[BF_4]^-$	Tetrafluoroborate
$[PF_6]^-$	Hexafluorophosphate
$[HSO_4]^-$	Hydrogen sulfate
$[DCA]^-$	Dicyanamide
$[Ac]^-$	Acetate
$[EtSO_4]^-$	Ethyl sulfate
$[MeSO_3]^-$	Methanesulfonate
$[DEP]^-$	Diethyl phosphate
$[MeO(H)PO_2]^-$	Methylphosphonate
$[FSI]^-$	Bis(fluorosulfonyl)imide
$[OTf]^-$	Trifluoromethanesulfonate
$[ESO_4]^-$	Ethyl sulfate
$[DMP]^-$	Dimethyl phosphate
$[OAc]^-$	Acetate
$[Lac]^-$	Lactate
$[ES]^-$	Ethyl sulfate
$[NTf_2]^-$	Bis(trifluoromethanesulfonyl)amide
$[DCA]^-$	Dicyanamide
$[OH]^-$	Hydroxide
$[Ch]^+$	Cholinium
$[EMIM]^+$	1-Ethyl-3-methylimidazolium
$[DEIM]^+$	1,2-Dimethyl-3-ethoxyethyl-imidazolium
$[BMIM]^+$	1-Butyl-3-methylimidazolium
$[C_6MIM]^+$	1-Hexyl-3-methylimidazolium
$[C_2MIM]^+$	1-Ethyl-3-methylimidazolium
$[VEIM]^+$	1-Vinyl-3-butylimidazolium

$[EtMeIM]^+$	1-Ethyl-3-methylimidazolium
$[(EtO)_3SiPMIM]^+$	3-Methyl-1-(3-(triethoxysilyl)propyl)-imidazolium
$[C_{18}C_1IM]^+$	1-Octadecyl-3-methylimidazolium
$[C_6C_1IM]^+$	1-Hexyl-3-methylimidazolium
$[C_4MPYR]^+$	*N*-Butyl-*N*-methylpyrrolidinium
$[CMMIM]^+$	1-Cyanomethyl-3-methylimidazolium
$[P_{66614}]^+$	Trihexyltetradecylphosphonium
$[P_{14}]^+$	1-Butyl-1-methylpyrrolidinium
$[Py_{13}]^+$	1-Methyl-1-propylpyrrolidinium
$[DMAEA\text{-}Q]^+$	Acryloyloxyethyltrimethylammonium
$[N_{4111}]^+$	Butyltrimethylammonium
$[PMEA\text{-}co\text{-}MTMA]^+$	Poly 2-methoxyethyl acrylate-*co*-[(2-(methacryloyloxy)ethyl)] trimethyl ammonium

Conflicts of interest

The authors declare no conflict of interest.

Acknowledgements

T.-P. L. thank the financial support from Distinguished University Professor grant (Nanyang Technological University), AcRF Tier 1 grants from the Ministry of Education of Singapore (RT14/20), and the Agency for Science, Technology and Research (A*STAR) under its MTC Individual Research Grant (M21K2c0114). Z. L. would like to express gratitude to the financial support from the Agency of Science, Technology and Research (A*STAR), Science and Engineering Research Council (SERC) Central Research Fund (Use-inspired Basic Research) for this work. X. F, Z. L. and T.-P. L. would also like to thank the A*STAR Research Grant support under RIE2025 Manufacturing, Trade and Connectivity (MTC) Programmatic Funding (M22K9b0049).

References

1 C. Ghobril and M. Grinstaff, *Chem. Soc. Rev.*, 2015, **44**, 1820–1835.
2 Y. Yi, C. Xie, J. Liu, Y. Zheng, J. Wang and X. Lu, *J. Mater. Chem. B*, 2021, **9**, 8739–8767.
3 X. Zhang, J. Xu, C. Lang, S. Qiao, G. An, X. Fan, L. Zhao, C. Hou and J. Liu, *Biomacromolecules*, 2017, **18**, 1885–1892.
4 P. C. Marr and A. C. Marr, *Green Chem.*, 2016, **18**, 105–128.
5 Y. S. Zhang and A. Khademhosseini, *Science*, 2017, **356**, eaaf3627.
6 Y. Guo, J. Bae, Z. Fang, P. Li, F. Zhao and G. Yu, *Chem. Rev.*, 2020, **120**, 7642–7707.
7 D. Wu, X. Li, J. Zheng, C. He, J. Zhang, Y. Xie, Y. Li, B. Tang, Y. Rui and F. Liu, *Electrochim. Acta*, 2021, **386**, 138334.
8 M. A. B. H. Susan, T. Kaneko, A. Noda and M. Watanabe, *J. Am. Chem. Soc.*, 2005, **127**, 4976–4983.
9 M.-A. Néouze, J. Le Bideau, F. Leroux and A. Vioux, *Chem. Commun.*, 2005, 1082–1084.
10 N. Chen, H. Zhang, L. Li, R. Chen and S. Guo, *Adv. Energy Mater.*, 2018, **8**, 1702675.
11 Y.-R. Gao, J.-F. Cao, Y. Shu and J.-H. Wang, *Green Chem. Eng.*, 2021, **2**, 368–383.
12 J. Saez, T. Glennon, M. Czugala, A. Tudor, J. Ducreé, D. Diamond, L. Florea and F. Benito-Lopez, *Sens. Actuators, B*, 2018, **257**, 963–970.
13 J. Le Bideau, J. B. Ducros, P. Soudan and D. Guyomard, *Adv. Funct. Mater.*, 2011, **21**, 4073–4078.
14 A. Guyomard-Lack, P. E. Delannoy, N. Dupré, C. V. Cerclier, B. Humbert and J. Le Bideau, *Phys. Chem. Chem. Phys.*, 2014, **16**, 23639–23645.
15 T. Shu, J. Wang, X. Li, X. Wang and S. Wang, *Electrochim. Acta*, 2023, **439**, 141656.
16 H. Li, Z. Feng, K. Zhao, Z. Wang, J. Liu, J. Liu and H. Song, *Nanoscale*, 2019, **11**, 3689–3700.
17 J. Zhang, E. Kamio, A. Matsuoka, K. Nakagawa, T. Yoshioka and H. Matsuyama, *J. Membr. Sci.*, 2022, **663**, 121032.
18 B. M. Lefler, W. M. Postiglione, C. Leighton and S. J. May, *Adv. Funct. Mater.*, 2022, **32**, 2208434.
19 X. Wu, S. Chen, M. Moser, A. Moudgil, S. Griggs, A. Marks, T. Li, I. McCulloch and W. L. Leong, *Adv. Funct. Mater.*, 2022, 2209354, DOI: 10.1002/adfm.202209354.
20 L. Porcarelli, J. L. Olmedo-Martinez, P. Sutton, V. Bocharova, A. Fdz De Anastro, M. Galceran, A. P. Sokolov, P. C. Howlett, M. Forsyth and D. Mecerreyes, *Gels*, 2022, **8**, 725.
21 J. Le Bideau, L. Viau and A. Vioux, *Chem. Soc. Rev.*, 2011, **40**, 907–925.
22 L. C. Tomé, L. Porcarelli, J. E. Bara, M. Forsyth and D. Mecerreyes, *Mater. Horiz.*, 2021, **8**, 3239–3265.
23 B. Kopilovic, F. A. e Silva, A. Q. Pedro, J. A. P. Coutinho and M. G. Freire, in *Nanotechnology for Biomedical Applications*, ed. S. Gopi, P. Balakrishnan and N. M. Mubarak, Springer Singapore, Singapore, 2022, pp. 391–425.
24 N. Jiang, X. Chang, D. Hu, L. Chen, Y. Wang, J. Chen and Y. Zhu, *Chem. Eng. J.*, 2021, **424**, 130418.
25 Q. Xu, Z. Zheng, B. Wang, H. Mao and F. Yan, *ACS Appl. Mater. Interfaces*, 2017, **9**, 14656–14664.
26 K. Peng, Y. Shi, A. LaBarbiera and S. Mitragotri, *ACS Biomater. Sci. Eng.*, 2020, DOI: 10.1021/acsbiomaterials.0c01024.
27 J.-Y. Jeon, S.-J. Park and T.-J. Ha, *Sens. Actuators, B*, 2022, **360**, 131672.
28 J. Zhang, E. Liu, S. Hao, X. Yang, T. Li, C. Lou, M. Run and H. Song, *Chem. Eng. J.*, 2022, **431**, 133949.
29 Z. Yu and P. Wu, *Adv. Funct. Mater.*, 2021, **31**, 2107226.
30 T. L. Greaves and C. J. Drummond, *Chem. Rev.*, 2015, **115**, 11379–11448.
31 S. Koutsoukos, J. Becker, A. Dobre, Z. Fan, F. Othman, F. Philippi, G. J. Smith and T. Welton, *Nat. Rev. Methods Primers*, 2022, **2**, 1–18.
32 J. M. S. S. Esperança, J. N. Canongia Lopes, M. Tariq, L. S. M. Santos, J. W. Magee and L. S. P. N. Rebelo, *J. Chem. Eng. Data*, 2010, **55**, 3–12.
33 K. S. Egorova, M. M. Seitkalieva, A. S. Kashin, E. G. Gordeev, A. V. Vavina, A. V. Posvyatenko and V. P. Ananikov, *J. Mol. Liq.*, 2022, **367**, 120450.

34 A. Brzęczek-Szafran, J. Więcławik, N. Barteczko, A. Szelwicka, E. Byrne, A. Kolanowska, M. S. Kwaśny and A. Chrobok, *Green Chem.*, 2021, **23**, 4421–4429.
35 T. Welton, *Biophys. Rev.*, 2018, **10**, 691–706.
36 R. Ratti, *Adv. Chem*, 2014, **2014**, 1–16.
37 A. J. Rennie, V. L. Martins, R. M. Torresi and P. J. Hall, *J. Phys. Chem. C*, 2015, **119**, 23865–23874.
38 Y. Prykhodko, A. Martin, H. Oulyadi, Y. L. Kobzar, S. Marais and K. Fatyeyeva, *J. Mol. Liq.*, 2022, **345**, 117782.
39 D. Zhao, M. Wu, Y. Kou and E. Min, *Catal. Today*, 2002, **74**, 157–189.
40 T. Wasilewski, J. Gębicki and W. Kamysz, *Trends Analyt. Chem.*, 2017, **93**, 23–36.
41 J. F. Wishart, *Energy Environ. Sci.*, 2009, **2**, 956–961.
42 S. K. Singh and A. W. Savoy, *J. Mol. Liq.*, 2020, **297**, 112038.
43 T.-P. Loh, L.-C. Feng, H.-Y. Yang and J.-Y. Yang, *Tetrahedron Lett.*, 2002, **43**, 8741–8743.
44 S.-L. Chen, S.-J. Ji and T.-P. Loh, *Tetrahedron Lett.*, 2003, **44**, 2405–2408.
45 S.-J. Ji, M.-F. Zhou, D.-G. Gu, S.-Y. Wang and T.-P. Loh, *Synlett*, 2003, 2077–2079.
46 S.-L. Chen, S.-J. Ji and T.-P. Loh, *Tetrahedron Lett.*, 2004, **45**, 375–377.
47 J. Lu, S.-J. Ji, R. Qian, J.-P. Chen, Y. Liu and T.-P. Loh, *Synlett*, 2004, 534–536.
48 S. J. Ji, M. F. Zhou, D. G. Gu, Z. Q. Jiang and T. P. Loh, *Eur. J. Org. Chem.*, 2004, 1584–1587.
49 S.-J. Ji, Z.-Q. Jiang, J. Lu and T.-P. Loh, *Synlett*, 2004, 0831–0835.
50 D.-G. Gu, S.-J. Ji, Z.-Q. Jiang, M.-F. Zhou and T.-P. Loh, *Synlett*, 2005, 0959–0962.
51 Z.-L. Shen, S.-J. Ji and T.-P. Loh, *Tetrahedron Lett.*, 2005, **46**, 3137–3139.
52 J. Lu, S.-J. Ji and T.-P. Loh, *Chem. Commun.*, 2005, 2345–2347.
53 Y.-C. Teo, E.-L. Goh and T.-P. Loh, *Tetrahedron Lett.*, 2005, **46**, 4573–4575.
54 J. Lu, S.-J. Ji, Y.-C. Teo and T.-P. Loh, *Tetrahedron Lett.*, 2005, **46**, 7435–7437.
55 F. Fu, Y.-C. Teo and T.-P. Loh, *Org. Lett.*, 2006, **8**, 5999–6001.
56 Z.-L. Shen, W.-J. Zhou, Y.-T. Liu, S.-J. Ji and T.-P. Loh, *Green Chem.*, 2008, **10**, 283–286.
57 J. F. Zhao, B. H. Tan, M. K. Zhu, T. B. W. Tjan and T. P. Loh, *Adv. Synth. Catal.*, 2010, **352**, 2085–2088.
58 Z.-L. Shen, K. K. K. Goh, C. H. A. Wong, W.-Y. Loo, Y.-S. Yang, J. Lu and T.-P. Loh, *Chem. Commun.*, 2012, **48**, 5856–5858.
59 Z.-L. Shen, H.-L. Cheong, Y.-C. Lai, W.-Y. Loo and T.-P. Loh, *Green Chem.*, 2012, **14**, 2626–2630.
60 B. A. da Silveira Neto, G. Ebeling, R. S. Gonçalves, F. C. Gozzo, M. N. Eberlin and J. Dupont, *Synthesis*, 2004, 1155–1158.
61 R. L. Vekariya, *J. Mol. Liq.*, 2017, **227**, 44–60.
62 M. Lijewski, J. M. Hogg, M. Swadźba-Kwaśny, P. Wasserscheid and M. Haumann, *RSC Adv.*, 2017, **7**, 27558–27563.
63 K. R. Seddon, *J. Chem. Technol. Biotechnol.*, 1997, **68**, 351–356.
64 J. S. Wilkes and M. J. Zaworotko, *J. Chem. Soc., Chem. Commun.*, 1992, 965–967.
65 W. Silva, M. Zanatta, A. S. Ferreira, M. C. Corvo and E. J. Cabrita, *Int. J. Mol. Sci.*, 2020, **21**, 7745.
66 J. H. Davis, *Chem. Lett.*, 2004, **33**, 1072–1077.
67 K. S. Egorova, E. G. Gordeev and V. P. Ananikov, *Chem. Rev.*, 2017, **117**, 7132–7189.
68 J. Gorke, F. Srienc and R. Kazlauskas, *Biotechnol. Bioprocess Eng.*, 2010, **15**, 40–53.
69 L. Ford, J. R. Harjani, F. Atefi, M. T. Garcia, R. D. Singer and P. J. Scammells, *Green Chem.*, 2010, **12**, 1783–1789.
70 N. Gathergood, P. J. Scammells and M. T. Garcia, *Green Chem.*, 2006, **8**, 156–160.
71 X.-D. Hou, Q.-P. Liu, T. J. Smith, N. Li and M.-H. Zong, *PLoS One*, 2013, **8**, e59145.
72 R. Boethling, E. Sommer and D. DiFiore, *Chem. Rev.*, 2007, **107**, 2207–2227.
73 N. Ferlin, M. Courty, S. Gatard, M. Spulak, B. Quilty, I. Beadham, M. Ghavre, A. Haiß, K. Kümmerer and N. Gathergood, *Tetrahedron*, 2013, **69**, 6150–6161.
74 M. Petkovic, J. L. Ferguson, H. Q. N. Gunaratne, R. Ferreira, M. C. Leitão, K. R. Seddon, L. P. N. Rebelo and C. S. Pereira, *Green Chem.*, 2010, **12**, 643–649.
75 J. Santos, A. Gonçalves, J. Pereira, B. Figueiredo, F. e Silva, J. Coutinho, S. Ventura and F. Gonçalves, *Green Chem.*, 2015, **17**, 4657–4668.
76 H. Ohno and K. Fukumoto, *Acc. Chem. Res.*, 2007, **40**, 1122–1129.
77 P. Wasserscheid and W. Keim, *Angew. Chem., Int. Ed.*, 2000, **39**, 3772–3789.
78 T. Welton, *Chem. Rev.*, 1999, **99**, 2071–2084.
79 C. P. Fredlake, J. M. Crosthwaite, D. G. Hert, S. N. Aki and J. F. Brennecke, *J. Chem. Eng. Data*, 2004, **49**, 954–964.
80 H. Shirota and E. W. Castner, *J. Phys. Chem. A*, 2005, **109**, 9388–9392.
81 J. W. Schmelzer, E. D. Zanotto and V. M. Fokin, *J. Chem. Phys.*, 2005, **122**, 074511.
82 F. Philippi, D. Rauber, K. L. Eliasen, N. Bouscharain, K. Niss, C. W. Kay and T. Welton, *Chem. Sci.*, 2022, **13**, 2735–2743.
83 R. Ludwig and U. Kragl, *Angew. Chem., Int. Ed.*, 2007, **46**, 6582–6584.
84 J. Vila, L. M. Varela and O. Cabeza, *Electrochim. Acta*, 2007, **52**, 7413–7417.
85 W. L. Yuan, X. Yang, L. He, Y. Xue, S. Qin and G. H. Tao, *Front. Chem.*, 2018, **6**, 59.
86 J. D. Holbrey, R. D. Rogers, R. A. Mantz, P. C. Trulove, V. A. Cocalia, A. E. Visser, J. L. Anderson, J. L. Anthony, J. F. Brennecke, E. J. Maginn, T. Welton and R. A. Mantz, in *Ionic Liquids in Synthesis*, ed. P. Wasserscheid and T. Welton, Wiley-VCH Verlag GmbH & Co. KGaA, 2008, pp. 57–174.
87 D. Rooney and J. Jacquemin, *Handbook of Solvents*, Elsevier, 2014, pp. 679–706.

88 T. Köddermann, C. Wertz, A. Heintz and R. Ludwig, *Angew. Chem., Int. Ed.*, 2006, **45**, 3697–3702.
89 N. Muhammad, Z. Man, A. K. Ziyada, M. A. Bustam, M. A. Mutalib, C. D. Wilfred, S. Rafiq and I. M. Tan, *J. Chem. Eng. Data*, 2012, **57**, 737–743.
90 Y. Cao and T. Mu, *Ind. Eng. Chem. Res.*, 2014, **53**, 8651–8664.
91 T. J. Wooster, K. M. Johanson, K. J. Fraser, D. R. MacFarlane and J. L. Scott, *Green Chem.*, 2006, **8**, 691–696.
92 P. Hapiot and C. Lagrost, *Chem. Rev.*, 2008, **108**, 2238–2264.
93 P. A. Suarez, C. S. Consorti, R. F. D. Souza, J. Dupont and R. S. Gonçalves, *J. Braz. Chem. Soc.*, 2002, **13**, 106–109.
94 M. Musiał, E. Zorębski, K. Malarz, M. Kuczak, A. Mrozek-Wilczkiewicz, J. Jacquemin and M. Dzida, *ACS Sustain. Chem. Eng.*, 2021, **9**, 7649–7657.
95 C. Zhang, L. Zhu, J. Wang, J. Wang, T. Zhou, Y. Xu and C. Cheng, *Ecotoxicol. Environ. Saf.*, 2017, **140**, 235–240.
96 S.-K. Ruokonen, C. Sanwald, M. Sundvik, S. Polnick, K. Vyavaharkar, F. Duša, A. J. Holding, A. W. T. King, I. Kilpeläinen, M. Lämmerhofer, P. Panula and S. K. Wiedmer, *Environ. Sci. Technol.*, 2016, **50**, 7116–7125.
97 N. Nikfarjam, M. Ghomi, T. Agarwal, M. Hassanpour, E. Sharifi, D. Khorsandi, M. Ali Khan, F. Rossi, A. Rossetti and E. Nazarzadeh Zare, *Adv. Funct. Mater.*, 2021, **31**, 2104148.
98 S. Stolte, J. Arning, U. Bottin-Weber, A. Müller, W.-R. Pitner, U. Welz-Biermann, B. Jastorff and J. Ranke, *Green Chem.*, 2007, **9**, 760–767.
99 S. A. Pérez, M. G. Montalbán, G. Carissimi, P. Licence and G. Víllora, *J. Hazard. Mater.*, 2020, **385**, 121513.
100 R. J. Bernot, M. A. Brueseke, M. A. Evans-White and G. A. Lamberti, *Environ. Toxicol. Chem.*, 2005, **24**, 87–92.
101 A. Borkowski, Ł. Ławniczak, T. Cłapa, D. Narożna, M. Selwet, D. Pęziak, B. Markiewicz and Ł. Chrzanowski, *Ecotoxicol. Environ. Saf.*, 2016, **130**, 54–64.
102 K. M. Docherty and J. C. F. Kulpa, *Green Chem.*, 2005, **7**, 185.
103 J. M. Gomes, S. S. Silva and R. L. Reis, *Chem. Soc. Rev.*, 2019, **48**, 4317–4335.
104 A. Foulet, O. B. Ghanem, M. El-Harbawi, J.-M. Lévêque, M. A. Mutalib and C.-Y. Yin, *J. Mol. Liq.*, 2016, **221**, 133–138.
105 D. K. Kaczmarek, D. Gwiazdowska, K. Juś, T. Klejdysz, M. Wojcieszak, K. Materna and J. Pernak, *New J. Chem.*, 2021, **45**, 6344–6355.
106 K. Fukumoto, M. Yoshizawa and H. Ohno, *J. Am. Chem. Soc.*, 2005, **127**, 2398–2399.
107 L. Zhang, L. He, C.-B. Hong, S. Qin and G.-H. Tao, *Green Chem.*, 2015, **17**, 5154–5163.
108 S. Kirchhecker, M. Antonietti and D. Esposito, *Green Chem.*, 2014, **16**, 3705–3709.
109 A. Jordan and N. Gathergood, *Chem. Soc. Rev.*, 2015, **44**, 8200–8237.
110 F. Boissou, A. Mühlbauer, K. D. O. Vigier, L. Leclercq, W. Kunz, S. Marinkovic, B. Estrine, V. Nardello-Rataj and F. Jérôme, *Green Chem.*, 2014, **16**, 2463–2471.
111 T. Michinobu, M. Hishida, M. Sato, Y. Katayama, E. Masai, M. Nakamura, Y. Otsuka, S. Ohara and K. Shigehara, *Polym. J.*, 2008, **40**, 68–75.
112 A. Romero, A. Santos, J. Tojo and A. Rodríguez, *J. Hazard. Mater.*, 2008, **151**, 268–273.
113 R. G. Gore, L. Myles, M. Spulak, I. Beadham, T. M. Garcia, S. J. Connon and N. Gathergood, *Green Chem.*, 2013, **15**, 2747–2760.
114 S. Stolte, S. Steudte, O. Areitioaurtena, F. Pagano, J. Thöming, P. Stepnowski and A. Igartua, *Chemosphere*, 2012, **89**, 1135–1141.
115 S. Stolte, T. Schulz, C.-W. Cho, J. Arning and T. Strassner, *ACS Sustain. Chem. Eng.*, 2013, **1**, 410–418.
116 B. Peric, J. Sierra, E. Martí, R. Cruañas, M. A. Garau, J. Arning, U. Bottin-Weber and S. Stolte, *J. Hazard. Mater.*, 2013, **261**, 99–105.
117 D. Coleman, M. Špulák, M. T. Garcia and N. Gathergood, *Green Chem.*, 2012, **14**, 1350–1356.
118 W. J. Hyun, C. M. Thomas and M. C. Hersam, *Adv. Energy Mater.*, 2020, **10**, 2002135.
119 M. Hoffmann, A. J. Butzelaar, C. Iacob, P. Theato and M. Wilhelm, *ACS Appl. Polym. Mater.*, 2022, **4**, 2794–2805.
120 D. M. Correia, L. C. Fernandes, P. M. Martins, C. García-Astrain, C. M. Costa, J. Reguera and S. Lanceros-Méndez, *Adv. Funct. Mater.*, 2020, **30**, 1909736.
121 K. Mishra, N. Devi, S. S. Siwal, Q. Zhang, W. F. Alsanie, F. Scarpa and V. K. Thakur, *Adv. Sci.*, 2022, **9**, 2202187.
122 R. Tamate, T. Ueki, A. M. Akimoto, R. Yoshida, T. Oyama, H. Kokubo and M. Watanabe, *RSC Adv.*, 2018, **8**, 3418–3422.
123 Y. Zhong, G. T. M. Nguyen, C. Plesse, F. Vidal and E. W. H. Jager, *J. Mater. Chem. C*, 2019, **7**, 256–266.
124 M. Sun, Z. Zeng, L. Peng, Z. Han, C. Yu, S. Cheng and J. Xie, *Mater. Today Energy*, 2021, **21**, 100785.
125 M. Zou, J. Luo, X. Wang, S. Tan, C. Wang and Y. Wu, *Ind. Eng. Chem. Res.*, 2021, **60**, 3589–3596.
126 S. Sultana, K. Ahmed, P. K. Jiwanti, B. Y. Wardhana and M. N. I. Shiblee, *Gels*, 2022, **8**, 2.
127 D. Aidoud, D. Guy-Bouyssou, D. Guyomard, J. Le Bideau and B. Lestriez, *ECS Trans.*, 2018, **86**, 163.
128 A. Guyomard-Lack, N. Buchtová, B. Humbert and J. Le Bideau, *Phys. Chem. Chem. Phys.*, 2015, **17**, 23947–23951.
129 T. P. Lodge and T. Ueki, *Acc. Chem. Res.*, 2016, **49**, 2107–2114.
130 C. Wang, K. Hashimoto, R. Tamate, H. Kokubo, K. Morishima, X. Li, M. Shibayama, F. Lu, T. Nakanishi and M. Watanabe, *Chem. Commun.*, 2019, **55**, 1710–1713.
131 J. Demarteau, A. Fernandez de Añastro, A. S. Shaplov and D. Mecerreyes, *Polym. Chem.*, 2020, **11**, 1481–1488.
132 K. Hashimoto, M. Hirasawa, H. Kokubo, R. Tamate, X. Li, M. Shibayama and M. Watanabe, *Macromolecules*, 2019, **52**, 8430–8439.
133 P. Bernardo, J. C. Jansen, F. Bazzarelli, F. Tasselli, A. Fuoco, K. Friess, P. Izák, V. Jarmarová, M. Kačírková and G. Clarizia, *Sep. Purif. Technol.*, 2012, **97**, 73–82.
134 S. S. Silva, J. F. Mano and R. L. Reis, *Green Chem.*, 2017, **19**, 1208–1220.

135 C. Hopson, M. M. Villar-Chavero, J. C. Domínguez, M. V. Alonso, M. Oliet and F. Rodriguez, *Carbohydr. Polym.*, 2021, **274**, 118663.
136 M. M. Villar-Chavero, J. C. Dominguez, M. V. Alonso, M. Oliet and F. Rodriguez, *Carbohydr. Polym.*, 2020, **229**, 115569.
137 A. Sharma, K. Rawat, P. R. Solanki and H. B. Bohidar, *Int. J. Biol. Macromol.*, 2017, **95**, 603–607.
138 W. P. Singh, U. Koch and R. S. Singh, *Soft Mater.*, 2020, **18**, 386–410.
139 Z. Chen, Q. Gui and Y. Wang, *Green Chem. Eng.*, 2021, **2**, 346–358.
140 L. Zhang, D. Jiang, T. Dong, R. Das, D. Pan, C. Sun, Z. Wu, Q. Zhang, C. Liu and Z. Guo, *Chem. Rec.*, 2020, **20**, 948–967.
141 J. Cui, Y. Li, D. Chen, T. G. Zhan and K. D. Zhang, *Adv. Funct. Mater.*, 2020, **30**, 2005522.
142 N. Kimizuka and T. Nakashima, *Langmuir*, 2001, **17**, 6759–6761.
143 A. Wu, F. Lu, P. Sun, X. Qiao, X. Gao and L. Zheng, *Langmuir*, 2017, **33**, 13982–13989.
144 S. Chen, N. Zhang, B. Zhang, B. Zhang and J. Song, *ACS Appl. Mater. Interfaces*, 2018, **10**, 44706–44715.
145 A. Maršavelski, V. Smrečki, R. Vianello, M. Žinić, A. Moguš-Milanković and A. Šantić, *Chem. – Eur. J.*, 2015, **21**, 12121–12128.
146 S. Dai, Y. H. Ju, H. J. Gao, J. S. Lin, S. J. Pennycook and C. E. Barnes, *Chem. Commun.*, 2000, 243–244.
147 M.-A. Néouze, J. L. Bideau, F. Leroux and A. Vioux, *Chem. Commun.*, 2005, 1082–1084, DOI: **10.1039/B416267F**.
148 K. G. Sharp, *J. Sol–Gel Sci. Technol.*, 1994, **2**, 35–41.
149 S. Thiemann, S. J. Sachnov, M. Gruber, F. Gannott, S. Spallek, M. Schweiger, J. Krückel, J. Kaschta, E. Spiecker, P. Wasserscheid and J. Zaumseil, *J. Mater. Chem. C*, 2014, **2**, 2423–2430.
150 A. K. Tripathi, *Mater. Today Energy*, 2021, **20**, 100643.
151 A. Guyomard-Lack, J. Abusleme, P. Soudan, B. Lestriez, D. Guyomard and J. L. Bideau, *Adv. Energy Mater.*, 2014, **4**, 1301570.
152 Z. He and P. Alexandridis, *Phys. Chem. Chem. Phys.*, 2015, **17**, 18238–18261.
153 S. Wang, B. Hsia, J. P. Alper, C. Carraro, Z. Wang and R. Maboudian, *J. Power Sources*, 2016, **301**, 299–305.
154 Q. Lyu, S. Wang, B. Peng, X. Chen, S. Du, M. Li, L. Zhang and J. Zhu, *Small*, 2021, **17**, e2103271.
155 A. Muñoz-Bonilla and M. Fernández-García, *Eur. Polym. J.*, 2018, **105**, 135–149.
156 W. Qian, J. Texter and F. Yan, *Chem. Soc. Rev.*, 2017, **46**, 1124–1159.
157 S.-Y. Zhang, Q. Zhuang, M. Zhang, H. Wang, Z. Gao, J.-K. Sun and J. Yuan, *Chem. Soc. Rev.*, 2020, **49**, 1726–1755.
158 I. Kammakakam, J. E. Bara and E. M. Jackson, *ACS Appl. Polym. Mater.*, 2020, **2**, 5067–5076.
159 H. Nakajima and H. Ohno, *Polymer*, 2005, **46**, 11499–11504.
160 P. Li, K. P. Pramoda and T.-S. Chung, *Ind. Eng. Chem. Res.*, 2011, **50**, 9344–9353.
161 S. Jeremias, M. Kunze, S. Passerini and M. Schonhoff, *J. Phys. Chem. B*, 2013, **117**, 10596–10602.
162 D. Zhou, R. Liu, J. Zhang, X. Qi, Y.-B. He, B. Li, Q.-H. Yang, Y.-S. Hu and F. Kang, *Nano Energy*, 2017, **33**, 45–54.
163 L. Ye, F. Chen, J. Liu, A. Gao, G. Kircher, W. Liu, M. Kappl, S. Wegner, H.-J. Butt and W. Steffen, *Macromol. Rapid Commun.*, 2019, **40**, 1900395.
164 Y. Ren, J. Guo, Z. Liu, Z. Sun, Y. Wu, L. Liu and F. Yan, *Sci. Adv.*, 2019, **5**, eaax0648.
165 C. M. Thomas, W. J. Hyun, H. C. Huang, D. Zeng and M. C. Hersam, *ACS Energy Lett.*, 2022, **7**, 1558–1565.
166 A. Vioux, L. Viau, S. Volland and J. Le Bideau, *C. R. Chim*, 2010, **13**, 242–255.
167 H. J. Kim, H. M. Yang, J. Koo, M. S. Kang, K. Hong and K. H. Lee, *ACS Appl. Mater. Interfaces*, 2017, **9**, 42978–42985.
168 J. H. Cho, J. Lee, Y. Xia, B. Kim, Y. He, M. J. Renn, T. P. Lodge and C. Daniel Frisbie, *Nat. Mat.*, 2008, **7**, 900–906.
169 J. Chen, F. Wang, G. Zhu, C. Wang, X. Cui, M. Xi, X. Chang and Y. Zhu, *ACS Appl. Mater. Interfaces*, 2021, **13**, 51567–51577.
170 D. Nevstrueva, K. Murashko, V. Vunder, A. Aabloo, A. Pihlajamäki, M. Mänttäri, J. Pyrhönen, T. Koiranen and J. Torop, *Colloids Surf., B*, 2018, **161**, 244–251.
171 Y. Wang, S. Sun and P. Wu, *Adv. Funct. Mater.*, 2021, **31**, 2101494.
172 B. Asbani, C. Douard, T. Brousse and J. Le Bideau, *Energy Stor. Mater*, 2019, **21**, 439–445.
173 L. C. Tomé, D. C. Guerreiro, R. M. Teodoro, V. D. Alves and I. M. Marrucho, *J. Membr. Sci.*, 2018, **549**, 267–274.
174 R. M. Teodoro, L. C. Tomé, D. Mantione, D. Mecerreyes and I. M. Marrucho, *J. Membr. Sci.*, 2018, **552**, 341–348.
175 L. C. Tomé, M. A. Aboudzadeh, L. P. N. Rebelo, C. S. R. Freire, D. Mecerreyes and I. M. Marrucho, *J. Mater. Chem. A*, 2013, **1**, 10403–10411.
176 D. Weng, F. Xu, X. Li, S. Li, Y. Li and J. Sun, *ACS Appl. Mater. Interfaces*, 2020, **12**, 57477–57485.
177 J. Sun, R. Li, G. Lu, Y. Yuan, X. Zhu and J. Nie, *J. Mater. Chem. C*, 2020, **8**, 8368–8373.
178 D. S. Ashby, R. H. DeBlock, C.-H. Lai, C. S. Choi and B. S. Dunn, *Joule*, 2017, **1**, 344–358.
179 G. D. Tabi, J. S. Kim, B. Nketia-Yawson, D. H. Kim and Y.-Y. Noh, *J. Mater. Chem. C*, 2020, **8**, 17107–17113.
180 P. E. Delannoy, B. Riou, T. Brousse, J. Le Bideau, D. Guyomard and B. Lestriez, *J. Power Sources*, 2015, **287**, 261–268.
181 L. Chen and M. Guo, *ACS Appl. Mater. Interfaces*, 2021, **13**, 25365–25373.
182 B. Asbani, B. Bounor, K. Robert, C. Douard, L. Athouël, C. Lethien, J. Le Bideau and T. Brousse, *J. Electrochem. Soc.*, 2020, **167**, 100551.
183 T. Guillemin, C. Douard, K. Robert, B. Asbani, C. Lethien, T. Brousse and J. Le Bideau, *Energy Stor. Mater*, 2022, **50**, 606–617.
184 S. Sert Çok, F. Koç, F. Balkan and N. Gizli, *J. Solid State Chem.*, 2019, **278**, 120877.
185 L. Viau, C. Tourné-Péteilh, J.-M. Devoisselle and A. Vioux, *Chem. Commun.*, 2010, **46**, 228–230.

186 K. Lunstroot, K. Driesen, P. Nockemann, C. Görller-Walrand, K. Binnemans, S. Bellayer, J. Le Bideau and A. Vioux, *Chem. Mater.*, 2006, **18**, 5711–5715.
187 Y. Wang, S. Kalytchuk, Y. Zhang, H. Shi, S. V. Kershaw and A. L. Rogach, *J. Phys. Chem. Lett.*, 2014, **5**, 1412–1420.
188 M.-A. Néouze, J. Le Bideau, P. Gaveau, S. Bellayer and A. Vioux, *Chem. Mater.*, 2006, **18**, 3931–3936.
189 K. G. Cho, H. J. Kim, H. M. Yang, K. H. Seol, S. J. Lee and K. H. Lee, *ACS Appl. Mater. Interfaces*, 2018, **10**, 40672–40680.
190 D. Lee, K. G. Cho, K. H. Seol, S. Lee, S.-H. Choi and K. H. Lee, *Org. Electron.*, 2019, **71**, 266–271.
191 T. Akyazi, J. Saez, J. Elizalde and F. Benito-Lopez, *Sens. Actuators, B*, 2016, **233**, 402–408.
192 J. T. Delaney Jr., A. R. Liberski, J. Perelaer and U. S. Schubert, *Macromol. Rapid Commun.*, 2010, **31**, 1970–1976.
193 M. Tijero, R. Díez-Ahedo, F. Benito-Lopez, L. Basabe-Desmonts, V. Castro-López and A. Valero, *Biomicrofluidics*, 2015, **9**, 044124.
194 B. Tang, D. K. Schneiderman, F. Zare Bidoky, C. D. Frisbie and T. P. Lodge, *ACS Macro Lett.*, 2017, **6**, 1083–1088.
195 A. Taubert, *Eur. J. Inorg. Chem.*, 2015, 1148–1159.
196 N. Jiang, H. Li, D. Hu, Y. Xu, Y. Hu, Y. Zhu, X. Han, G. Zhao, J. Chen, X. Chang, M. Xi and Q. Yuan, *Compos. Commun.*, 2021, **27**, 100845.
197 J. Wong, A. T. Gong, P. A. Defnet, L. Meabe, B. Beauchamp, R. M. Sweet, H. Sardon, C. L. Cobb and A. Nelson, *Adv. Mater. Technol.*, 2019, **4**, 1900452.
198 G. C. Luque, M. L. Picchio, A. P. S. Martins, A. Dominguez-Alfaro, N. Ramos, I. del Agua, B. Marchiori, D. Mecerreyes, R. J. Minari and L. C. Tomé, *Adv. Electron. Mater.*, 2021, **7**, 2100178.
199 Y. Shi, Y. Wang, Y. Gu, L. Zheng, S. Ma and X. Xu, *Chem. Eng. J.*, 2020, **392**, 123645.
200 S. Hao, T. Li, X. Yang and H. Song, *ACS Appl. Mater. Interfaces*, 2022, **14**, 2029–2037.
201 Z. Wang, J. Zhang, J. Liu, S. Hao, H. Song and J. Zhang, *ACS Appl. Mater. Interfaces*, 2021, **13**, 5614–5624.
202 K. Ahmed, N. Naga, M. Kawakami and H. Furukawa, *Macromol. Chem. Phys.*, 2018, **219**, 1800216.
203 A. Basu, J. Wong, B. Cao, N. Boechler, A. J. Boydston and A. Nelson, *ACS Appl. Mater. Interfaces*, 2021, **13**, 19263–19270.
204 M. Wang, P. Zhang, M. Shamsi, J. L. Thelen, W. Qian, V. K. Truong, J. Ma, J. Hu and M. D. Dickey, *Nat. Mater.*, 2022, **21**, 359–365.
205 Y. Gao, J. Guo, J. Chen, G. Yang, L. Shi, S. Lu, H. Wu, H. Mao, X. Da, G. Gao and S. Ding, *Chem. Eng. J.*, 2022, **427**, 131057.
206 P. Guo, A. Su, Y. Wei, X. Liu, Y. Li, F. Guo, J. Li, Z. Hu and J. Sun, *ACS Appl. Mater. Interfaces*, 2019, **11**, 19413–19420.
207 D. Zhao, Y. Zhu, W. Cheng, G. Xu, Q. Wang, S. Liu, J. Li, C. Chen, H. Yu and L. Hu, *Matter*, 2020, **2**, 390–403.
208 Y. Wang, Y. Liu, R. Plamthottam, M. Tebyetekerwa, J. Xu, J. Zhu, C. Zhang and T. Liu, *Macromolecules*, 2021, **54**, 3832–3844.
209 S. Hao, J. Zhang, X. Yang, T. Li and H. Song, *J. Mater. Chem. C*, 2021, **9**, 5789–5799.
210 Z. Lei and P. Wu, *Nat. Commun.*, 2019, **10**, 3429.
211 Z. Cao, H. Liu and L. Jiang, *Mater. Horiz.*, 2020, **7**, 912–918.
212 L. M. Zhang, Y. He, S. Cheng, H. Sheng, K. Dai, W. J. Zheng, M. X. Wang, Z. S. Chen, Y. M. Chen and Z. Suo, *Small*, 2019, **15**, 1804651.
213 Y. M. Kim and H. C. Moon, *Adv. Funct. Mater.*, 2020, **30**, 1907290.
214 W. Qiu, G. Chen, H. Zhu, Q. Zhang and S. Zhu, *Chem. Eng. J.*, 2022, **434**, 134752.
215 J. Sun, G. Lu, J. Zhou, Y. Yuan, X. Zhu and J. Nie, *ACS Appl. Mater. Interfaces*, 2020, **12**, 14272–14279.
216 Q. Xia, W. Li, X. Zou, S. Zheng, Z. Liu, L. Li and F. Yan, *Mater. Horiz.*, 2022, **9**, 2881–2892.
217 L. Xu, Z. Huang, Z. Deng, Z. Du, T. L. Sun, Z.-H. Guo and K. Yue, *Adv. Mater.*, 2021, **33**, 2105306.
218 P. Shi, Y. Wang, W. W. Tjiu, C. Zhang and T. Liu, *ACS Appl. Mater. Interfaces*, 2021, **13**, 49358–49368.
219 R. Tamate, K. Hashimoto, X. Li, M. Shibayama and M. Watanabe, *Polymer*, 2019, **178**, 121694.
220 I. Osada, H. de Vries, B. Scrosati and S. Passerini, *Angew. Chem., Int. Ed.*, 2016, **55**, 500–513.
221 M. Chen, B. T. White, C. R. Kasprzak and T. E. Long, *Eur. Polym. J.*, 2018, **108**, 28–37.
222 J. Yuan, D. Mecerreyes and M. Antonietti, *Prog. Polym. Sci.*, 2013, **38**, 1009–1036.
223 S. A. M. Noor, P. M. Bayley, M. Forsyth and D. R. MacFarlane, *Electrochim. Acta*, 2013, **91**, 219–226.
224 Z. Luo, W. Li, J. Yan and J. Sun, *Adv. Funct. Mater.*, 2022, **32**, 2203988.
225 K. Liu, J. Lv, G. Fan, B. Wang, Z. Mao, X. Sui and X. Feng, *Adv. Funct. Mater.*, 2022, **32**, 2107105.
226 Y. Ding, J. Zhang, L. Chang, X. Zhang, H. Liu and L. Jiang, *Adv. Mater.*, 2017, **29**, 1704253.
227 K. Shahzadi, W. Xiong, M. Shekh, F. J. Stadler and Z.-C. Yan, *ACS Appl. Mater. Interfaces*, 2020, **12**, 49050–49060.
228 J. Lan, Y. Li, B. Yan, C. Yin, R. Ran and L.-Y. Shi, *ACS Appl. Mater. Interfaces*, 2020, **12**, 37597–37606.
229 J. Sun, Y. Yuan, G. Lu, L. Li, X. Zhu and J. Nie, *J. Mater. Chem. C*, 2019, **7**, 11244–11250.
230 B. Yiming, X. Guo, N. Ali, N. Zhang, X. Zhang, Z. Han, Y. Lu, Z. Wu, X. Fan, Z. Jia and S. Qu, *Adv. Funct. Mater.*, 2021, **31**, 2102773.
231 Y. Ren, Z. Liu, G. Jin, M. Yang, Y. Shao, W. Li, Y. Wu, L. Liu and F. Yan, *Adv. Mater.*, 2021, **33**, 2008486.
232 L. Zhang, K. Jia, J. Wang, J. Zhao, J. Tang and J. Hu, *Mater. Horiz.*, 2022, 1911–1920, DOI: **10.1039/D1MH01775F**.
233 C. Xu and Z. Cheng, *Processes*, 2021, **9**, 337.
234 J.-K. Kim, J. Scheers, T. J. Park and Y. Kim, *ChemSusChem*, 2015, **8**, 636–641.
235 F. Wu, N. Chen, R. Chen, L. Wang and L. Li, *Nano Energy*, 2017, **31**, 9–18.
236 Y. Lu, S. S. Moganty, J. L. Schaefer and L. A. Archer, *J. Mater. Chem.*, 2012, **22**, 4066–4072.

237 Y. Lu, S. K. Das, S. S. Moganty and L. A. Archer, *Adv. Mater.*, 2012, **24**, 4430–4435.
238 A. I. Horowitz and M. J. Panzer, *J. Mater. Chem.*, 2012, **22**, 16534–16539.
239 J. Le Bideau, P. Gaveau, S. Bellayer, M. A. Néouze and A. Vioux, *Phys. Chem. Chem. Phys.*, 2007, **9**, 5419–5422.
240 J. Xu, H. Wang, X. Du, X. Cheng, Z. Du and H. Wang, *Chem. Eng. J.*, 2021, **426**, 130724.
241 Q. Xia, J. Wu, Q. X. Shi, X. Xiang, X. Li, H. Pei, H. Zeng, X. Xie and Y. S. Ye, *J. Power Sources*, 2019, **414**, 283–292.
242 P. Raut, W. Liang, Y.-M. Chen, Y. Zhu and S. C. Jana, *ACS Appl. Mater. Interfaces*, 2017, **9**, 30933–30942.
243 G. Tan, F. Wu, C. Zhan, J. Wang, D. Mu, J. Lu and K. Amine, *Nano Lett.*, 2016, **16**, 1960–1968.
244 W. J. Hyun, A. C. M. de Moraes, J.-M. Lim, J. R. Downing, K.-Y. Park, M. T. Z. Tan and M. C. Hersam, *ACS Nano*, 2019, **13**, 9664–9672.
245 J. W. Suen, N. K. Elumalai, S. Debnath, N. M. Mubarak, C. I. Lim and M. M. Reddy, *Adv. Mater. Interfaces*, 2022, **9**, 2201405.
246 F. Wu, N. Chen, R. Chen, Q. Zhu, G. Tan and L. Li, *Adv. Sci.*, 2016, **3**, 1500306.
247 M. Isik, R. Gracia, L. C. Kollnus, L. C. Tomé, I. M. Marrucho and D. Mecerreyes, *ACS Macro Lett.*, 2013, **2**, 975–979.
248 H. Zhang, X. Yu, Y. Wang, X. Fan, Y.-E. Miao, X. Zhang and T. Liu, *Compos. Sci. Technol.*, 2022, **230**, 109740.
249 L. Migliorini, C. Piazzoni, K. Pohako-Esko, M. Di Girolamo, A. Vitaloni, F. Borghi, T. Santaniello, A. Aabloo and P. Milani, *Adv. Funct. Mater.*, 2021, **31**, 2102180.
250 H. Li, F. Xu, T. Guan, Y. Li and J. Sun, *Nano Energy*, 2021, **90**, 106645.
251 M. Zhang, X. Tao, R. Yu, Y. He, X. Li, X. Chen and W. Huang, *J. Mater. Chem. A*, 2022, **10**, 12005–12015.
252 H. Wang, J. Xu, K. Li, Y. Dong, Z. Du and S. Wang, *J. Mater. Chem. B*, 2022, **10**, 1301–1307.
253 S. Zhuo, C. Song, Q. Rong, T. Zhao and M. Liu, *Nat. Commun.*, 2022, **13**, 1743.
254 K. Lunstroot, K. Driesen, P. Nockemann, K. Van Hecke, L. Van Meervelt, C. Görller-Walrand, K. Binnemans, S. Bellayer, L. Viau, J. Le Bideau and A. Vioux, *Dalton Trans.*, 2009, 298–306, DOI: 10.1039/B812292J.
255 X. Li, Q. Li, N. Lei and X. Chen, *ACS Omega*, 2019, **4**, 2437–2444.
256 G. Singh, G. Singh, K. Damarla, P. K. Sharma, A. Kumar and T. S. Kang, *ACS Sustain. Chem. Eng.*, 2017, **5**, 6568–6577.
257 L. C. Tomé, N. H. C. S. Silva, H. R. Soares, A. S. Coroadinha, P. Sadocco, I. M. Marrucho and C. S. R. Freire, *Green Chem.*, 2015, **17**, 4291–4299.
258 L. Poletti, C. Chiappe, L. Lay, D. Pieraccini, L. Polito and G. Russo, *Green Chem.*, 2007, **9**, 337–341.
259 M. Isik, T. Lonjaret, H. Sardon, R. Marcilla, T. Herve, G. G. Malliaras, E. Ismailova and D. Mecerreyes, *J. Mater. Chem. C*, 2015, **3**, 8942–8948.
260 E. Bihar, T. Roberts, E. Ismailova, M. Saadaoui, M. Isik, A. Sanchez-Sanchez, D. Mecerreyes, T. Hervé, J. B. De Graaf and G. G. Malliaras, *Adv. Mater. Technol.*, 2017, **2**, 1600251.
261 M. M. Villar-Chavero, J. C. Domínguez, M. V. Alonso, V. Rigual, M. Oliet and F. Rodriguez, *Int. J. Biol. Macromol.*, 2019, **133**, 262–269.
262 Z. Wang, J. Liu, J. Zhang, S. Hao, X. Duan, H. Song and J. Zhang, *Cellulose*, 2020, **27**, 5121–5133.
263 D. Coleman and N. Gathergood, *Chem. Soc. Rev.*, 2010, **39**, 600–637.
264 M. J. Mehta and A. Kumar, *ACS Sustain. Chem. Eng.*, 2019, **7**, 8631–8636.
265 Z.-L. Xie, H.-B. Xu, A. Geßner, M. U. Kumke, M. Priebe, K. M. Fromm and A. Taubert, *J. Mater. Chem.*, 2012, **22**, 8110–8116.
266 Q. Feng, K. Wan, T. Zhu, C. Zhang and T. Liu, *Chem. Eng. J.*, 2022, **435**, 134826.
267 Z. Qiu, Y. Wan, W. Zhou, J. Yang, J. Yang, J. Huang, J. Zhang, Q. Liu, S. Huang, N. Bai, Z. Wu, W. Hong, H. Wang and C. F. Guo, *Adv. Funct. Mater.*, 2018, **28**, 1802343.
268 T. Li, Y. Wang, S. Li, X. Liu and J. Sun, *Adv. Mater.*, 2020, **32**, 2002706.
269 K. G. Cho, S. An, D. H. Cho, J. H. Kim, J. Nam, M. Kim and K. H. Lee, *Adv. Funct. Mater.*, 2021, **31**, 2102386.
270 L. Ma, J. Wang, J. He, Y. Yao, X. Zhu, L. Peng, J. Yang, X. Liu and M. Qu, *J. Mater. Chem. A*, 2021, **9**, 26949–26962.
271 L. Zhao, B. Wang, Z. Mao, X. Sui and X. Feng, *Chem. Eng. J.*, 2022, **433**, 133500.
272 Y. Xu, L. Chen, J. Chen, X. Chang and Y. Zhu, *ACS Appl. Mater. Interfaces*, 2022, **14**, 2122–2131.
273 J. Yang, Q. Liu, Z. Deng, M. Gong, F. Lei, J. Zhang, X. Zhang, Q. Wang, Y. Liu, Z. Wu and C. F. Guo, *Mater. Today Phys.*, 2019, **8**, 78–85.
274 F. Wang, S. Zhang, Y. Zhang, Q. Lin, Y. Chen, D. Zhu, L. Sun and T. Chen, *Nanomaterials*, 2019, **9**, 343.
275 A. Y. Yuen, L. Porcarelli, R. H. Aguirresarobe, A. Sanchez-Sanchez, I. Del Agua, U. Ismailov, G. G. Malliaras, D. Mecerreyes, E. Ismailova and H. Sardon, *Polymers*, 2018, **10**, 989.
276 S. Xiao, J. Nie, R. Tan, X. Duan, J. Ma, Q. Li and T. Wang, *Mater. Chem. Front.*, 2019, **3**, 484–491.
277 J. Dai, X. Guan, H. Zhao, S. Liu, T. Fei and T. Zhang, *Sens. Actuators, B*, 2020, **316**, 128159.
278 S. Xiang, X. He, F. Zheng and Q. Lu, *Chem. Eng. J.*, 2022, **439**, 135644.
279 V. Amoli, J. S. Kim, E. Jee, Y. S. Chung, S. Y. Kim, J. Koo, H. Choi, Y. Kim and D. H. Kim, *Nat. Commun.*, 2019, **10**, 4019.
280 J. Wang, J. Xu, T. Chen, L. Song, Y. Zhang, Q. Lin, M. Wang, F. Wang, N. Ma and L. Sun, *Sens. Actuator A Phys.*, 2021, **321**, 112583.
281 L. Sun, S. Chen, Y. Guo, J. Song, L. Zhang, L. Xiao, Q. Guan and Z. You, *Nano Energy*, 2019, **63**, 103847.
282 C. He, S. Sun and P. Wu, *Mater. Horiz.*, 2021, **8**, 2088–2096.
283 M. Mokhtarpour, H. Shekaari and A. Shayanfar, *J. Drug Deliv. Sci. Technol.*, 2020, **56**, 101512.
284 M. Kuddushi, N. K. Patel, S. Rajput, O. A. El Seoud, J. P. Mata and N. I. Malek, *ChemSystemsChem*, 2020, **2**, 1900053.

285 J. N. Pendleton and B. F. Gilmore, *Int. J. Antimicrob. Agents*, 2015, **46**, 131–139.
286 E. R. D. Seiler, K. Koyama, T. Iijima, T. Saito, Y. Takeoka, M. Rikukawa and M. Yoshizawa-Fujita, *Polymers*, 2021, **13**, 1942.
287 J. Guo, Y. Qian, B. Sun, Z. Sun, Z. Chen, H. Mao, B. Wang and F. Yan, *ACS Appl. Bio Mater.*, 2019, **2**, 4418–4426.
288 Z. Luo, H. Cui, J. Guo, J. Yao, X. Fang, F. Yan, B. Wang and H. Mao, *Adv. Funct. Mater.*, 2021, **31**, 2100336.
289 H. A. Yu, J. Lee, S. W. Lewis and D. S. Silvester, *Anal. Chem.*, 2017, **89**, 4729–4736.
290 Y. Lu, J. Hu, Y. Zeng, Y. Zhu, H. Wang, X. Lei, S. Huang, L. Guo and L. Li, *Sens. Actuators, B*, 2020, **311**, 127911.
291 F. Valentini, D. Roscioli, M. Carbone, V. Conte, B. Floris, E. M. Bauer, N. Ditaranto, L. Sabbatini, E. Caponetti and D. Chillura-Martino, *Sens. Actuators, B*, 2015, **212**, 248–255.
292 X. Zhang, *Int. J. Electrochem.*, 2020, **15**, 9179–9190.
293 S. Doblinger, C. E. Hay, L. C. Tome, D. Mecerreyes and D. S. Silvester, *Anal. Chim. Acta*, 2022, **1195**, 339414.
294 W. B. Gonçalves, E. P. Cervantes, A. C. C. S. Pádua, G. Santos, S. I. C. J. Palma, R. W. C. Li, A. C. A. Roque and J. Gruber, *Chemosensors*, 2021, **9**, 201.